RESEARCH ARTICLE

Design and Efficacy of a Monovalent Bispecific PD-1/CTLA4 Antibody That Enhances CTLA4 Blockade on PD-1$^+$ Activated T Cells

Simon J. Dovedi[1], Matthew J. Elder[1], Chunning Yang[2], Suzanne I. Sitnikova[1], Lorraine Irving[2], Anna Hansen[3], James Hair[1], Des C. Jones[1], Sumati Hasani[2], Bo Wang[2], Seock-Ah Im[4], Ben Tran[5], Deepa S. Subramaniam[1], Shelby D. Gainer[1], Kapil Vashisht[6], Arthur Lewis[1], Xiaofang Jin[2], Stacy Kentner[1], Kathy Mulgrew[1], Yaya Wang[1], Michael G. Overstreet[1], James Dodgson[2], Yanli Wu[2], Asis Palazon[1], Michelle Morrow[1], Godfrey J. Rainey[2], Gareth J. Browne[2], Frances Neal[2], Thomas V. Murray[2], Aleksandra D. Toloczko[2], William Dall'Acqua[2], Ikbel Achour[1], Daniel J. Freeman[1], Robert W. Wilkinson[1], and Yariv Mazor[2]

ABSTRACT

The clinical benefit of PD-1 blockade can be improved by combination with CTLA4 inhibition but is commensurate with significant immune-related adverse events suboptimally limiting the doses of anti-CTLA4 mAb that can be used. MEDI5752 is a monovalent bispecific antibody designed to suppress the PD-1 pathway and provide modulated CTLA4 inhibition favoring enhanced blockade on PD-1$^+$ activated T cells. We show that MEDI5752 preferentially saturates CTLA4 on PD-1$^+$ T cells versus PD-1$^-$ T cells, reducing the dose required to elicit IL2 secretion. Unlike conventional PD-1/CTLA4 mAbs, MEDI5752 leads to the rapid internalization and degradation of PD-1. Moreover, we show that MEDI5752 preferentially localizes and accumulates in tumors providing enhanced activity when compared with a combination of mAbs targeting PD-1 and CTLA4 *in vivo*. Following treatment with MEDI5752, robust partial responses were observed in two patients with advanced solid tumors. MEDI5752 represents a novel immunotherapy engineered to preferentially inhibit CTLA4 on PD-1$^+$ T cells.

SIGNIFICANCE: The unique characteristics of MEDI5752 represent a novel immunotherapy engineered to direct CTLA4 inhibition to PD-1$^+$ T cells with the potential for differentiated activity when compared with current conventional mAb combination strategies targeting PD-1 and CTLA4. This molecule therefore represents a step forward in the rational design of cancer immunotherapy.

See related commentary by Burton and Tawbi, p. 1008.

[1]Early Oncology R&D, AstraZeneca. [2]Antibody Discovery and Protein Engineering, R&D, AstraZeneca. [3]Translational Science and Experimental Medicine, Respiratory and Immunology (RI), Biopharmaceuticals R&D, AstraZeneca. [4]Division of Hematology-Oncology, Department of Internal Medicine, Seoul National University Hospital, Seoul National University School of Medicine, Seoul, Korea. [5]Department of Medical Oncology, Peter MacCallum Cancer Centre, Melbourne, Australia. [6]Clinical Pharmacology & Safety Sciences, AstraZeneca.

Note: Supplementary data for this article are available at Cancer Discovery Online (http://cancerdiscovery.aacrjournals.org/).

S.J. Dovedi and Y. Mazor contributed equally to this article.

Corresponding Authors: Simon J. Dovedi, Early Oncology R&D, AstraZeneca, Aaron Klug Building, Granta Park, Cambridge CB21 6GH, UK. E-mail: simon.dovedi@astrazeneca.com; and Yariv Mazor, Antibody Discovery and Protein Engineering, R&D, AstraZeneca, Gaithersburg, MD 20878. E-mail: yariv.mazor@astrazeneca.com

Cancer Discov 2021;11:1100–17

doi: 10.1158/2159-8290.CD-20-1445

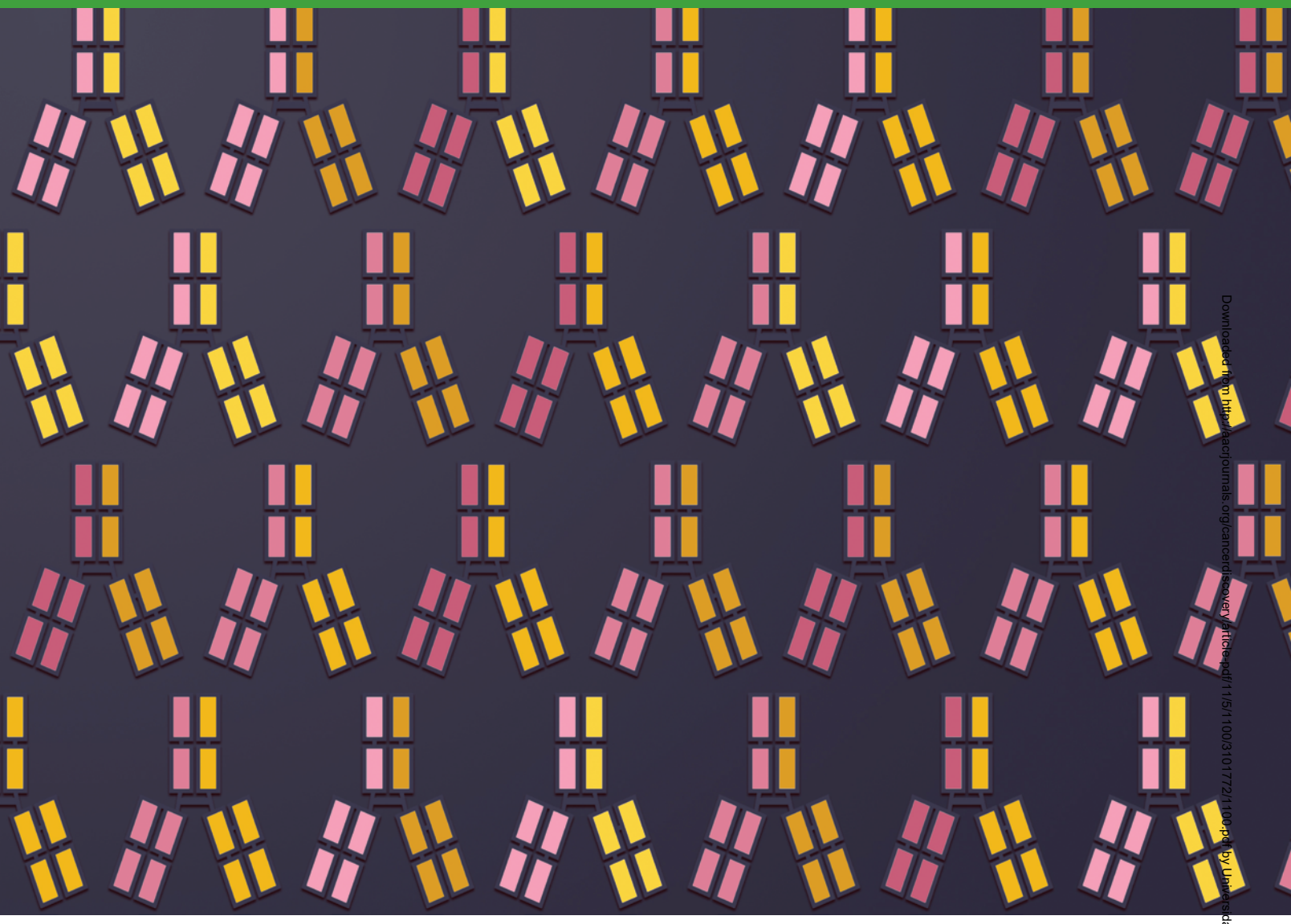

INTRODUCTION

Immune checkpoint blockade (ICB) is now an established part of the standard of care for a broad range of tumor types (1). To date, regulatory approvals center on two key coinhibitory pathways: PD-1 and CTLA4 (2). Moreover, a combination of PD-1 and CTLA4 blockade has been shown to improve overall survival and is approved for the treatment of advanced melanoma, renal cell carcinoma (RCC), and non–small cell lung cancer (NSCLC; refs. 3–6). However, although a dose-dependent response has been observed clinically for anti-CTLA4 mAb, the therapeutic dose is limited due to immune-related adverse events (irAE; refs. 7, 8). Therefore, novel approaches to facilitate enhanced CTLA4 blockade, in combination with a PD-1 mAb, are urgently needed.

The coinhibitory molecule PD-1 is induced following T-cell activation with expression maintained via repeated signaling through the T-cell receptor (TCR). As a consequence, PD-1 is a marker of tumor-associated antigen–specific tumor-infiltrating lymphocytes (TIL; ref. 9). Signaling through PD-1 via binding to PD-L1 and PD-L2 can negatively regulate T-cell responses both by attenuating TCR signaling (10, 11) and through dephosphorylation of the costimulatory receptor CD28 (12, 13). Blockade of this signaling axis leads to reinvigoration of T-cell function and effective antitumor responses.

CTLA4 is a coinhibitory molecule that is rapidly upregulated following TCR engagement (14). CTLA4 binds to the coactivatory receptors CD80 and CD86 expressed on antigen-presenting cells with higher affinity than CD28, thereby regulating T-cell activation and function via modulation of the amplitude of signaling through the TCR/MHC complex (15–20). In addition, CTLA4 can also function through a cell-extrinsic mechanism by limiting the availability of CD80/CD86 either through competition or by ligand transendocytosis, owing to the rapid turnover of the receptor from the plasma membrane to intracellular vesicles (21). CTLA4 expression is elevated on tumor-infiltrating regulatory T cells (Treg) and on subpopulations of antigen-experienced/exhausted effector T (Teff) cells when compared

with peripheral T-cell populations (22–24). Therefore, CTLA4 functions to regulate the provision of costimulatory signaling through CD28, affecting both initial T-cell priming and activity of antigen-experienced T cells (16, 24, 25).

Interestingly, previous studies have demonstrated that tumor-resident PD-1$^+$ effector memory T cells are associated with response to PD-1 monotherapy and combined PD-1/CTLA4 therapy (26, 27). Moreover, several preclinical studies demonstrate that local administration of anti-CTLA4 mAb into the tumor or administration of a prodrug that is rendered active in the tumor microenvironment (TME) is sufficient for mediating antitumor activity and is commensurate with reduced peripheral immune activation versus systemic administration and may therefore be used in an attempt to uncouple antitumor activity from potential irAEs (28–36). Supporting this, early diversification of the TCR repertoire following CTLA4 blockade has been associated with irAEs, suggesting that peripheral blockade of this pathway may contribute to its toxicity profile through the activation of new T-cell clones (37, 38).

MEDI5752 has been designed to suppress signaling through the PD-1 axis and provide preferential inhibition of CTLA4 on activated PD-1$^+$ T cells when compared with PD-1$^-$ T-cell populations. Here, we show that MEDI5752 can saturate CTLA4 on PD-1$^+$ cells at orders of magnitude lower concentrations than required to saturate CTLA4 on PD-1$^-$ cells. Specifically, in a range of *in vitro* assays, we show that MEDI5752 can enhance T-cell activity when compared with a combination of mAbs targeting the PD-1 and CTLA4 pathways. Furthermore, when compared with a combination of mAbs, we show that MEDI5752 can preferentially accumulate in the TME and generate effective antitumor immune responses in humanized mice. Moreover, we show that by tethering CTLA4 to PD-1, MEDI5752 leads to the internalization and subsequent degradation of PD-1. Collectively, these novel mechanisms of action may allow for effective blockade of the PD-1 axis while providing enhanced CTLA4 inhibition in the TME than can be achieved versus conventional mAb-based combinatorial approaches. To support the translational nature of our work, we present illustrative evidence of clinical activity in two patients treated with MEDI5752 from an ongoing phase I study in advanced solid tumors (NCT03530397).

RESULTS

Expression of CTLA4 on TILs Is Enriched on PD-1$^+$ T Cells across a Range of Solid Tumors

PD-1 and CTLA4 expression on TILs from 44 disaggregated tumors (ICB-naïve) across four indications (colorectal cancer, NSCLC, RCC, and melanoma) were profiled by flow cytometry. These data revealed that PD-1/CTLA4 double-positive CD4$^+$ and CD8$^+$ T cells could be found across all tumor types and that expression of CTLA4 was enriched on PD-1$^+$ T cells (Fig. 1A and B; Supplementary Fig. S1A and S1B). Moreover, we show that CD39 expression, a marker for tumor-reactive CD8$^+$ T cells (39), was enriched on these PD-1$^+$CTLA4$^+$ TILs (Fig. 1C). We then used coregistrational analysis on sequential tissue sections to further interrogate PD-1 and CTLA4 expression on TILs from 183 tumors across squamous cell carcinoma of the head and neck (SCCHN), NSCLC, and urothelial cell carcinoma (UCC). These data demonstrated that 80% SCCHN, 84% squamous cell NSCLC, 89% adenocarcinoma NSCLC, and 90% UCC profiled in these indications are infiltrated by TILs coexpressing PD-1 and CTLA4 (Fig. 1D and E). Based on these expression data, we generated a novel bispecific antibody that could cotarget PD-1 and CTLA4.

Design and Characterization of a Monovalent Bispecific Antibody Targeting PD-1 and CTLA4

The variable domains of tremelimumab (anti-CTLA4) and an anti–PD-1 mAb were formatted onto a DuetMab backbone (40). The human gamma-1 constant heavy chain was further engineered to carry the triple mutations (L234F, L235E, and P331S) designed to reduce fragment crystallizable (Fc)–mediated immune effector functions (41). The corresponding anti–PD-1/CTLA4 monovalent bispecific DuetMab was designated MEDI5752. The intrinsic binding kinetics of MEDI5752 for recombinant human, cynomolgus monkey, and murine PD-1 and CTLA4 antigens were determined by surface plasmon resonance. The PD-1 and CTLA4 arms of MEDI5752 maintain the intrinsic binding affinity of the parental mAbs from which they were derived. Consistent with the binding properties of the two parental mAbs, MEDI5752 exhibits only residual binding to the murine ortholog of PD-1 and shows no cross-reactivity to murine CTLA4 (Supplementary Fig. S2). The ability of MEDI5752 to concurrently bind recombinant human and cynomolgus monkey PD-1 and CTLA4 proteins was determined by Octet analysis (Supplementary Fig. S3A and S3B). Guided by expression data from TILs (Supplementary Fig. S4), we generated engineered Chinese hamster ovary (CHO) cell lines expressing either PD-1, CTLA4, or a combination of receptors where PD-1 was in approximately 10- or 40-fold excess *cf.* CTLA4 (Supplementary Fig. S5). We show that MEDI5752 maintains the binding properties of parental anti–PD-1 and anti-CTLA4 mAbs to their respective target receptors on CHO cells (Supplementary Fig. S6A–S6D) and on stimulated CD4$^+$ and CD8$^+$ T cells (Supplementary Fig. S7A–S7D). We then confirmed that MEDI5752 was able to concurrently bind PD-1 and CTLA4 receptors on the surface of the same cell and thereby was able to mediate cross-arm avidity binding (Supplementary Fig. S8A and S8B).

Valence Affects CTLA4 Inhibition but Has Minimal Impact on PD-1

We determined how valence would affect PD-1 and CTLA4 receptor inhibition using two-cell luciferase reporter

Figure 1. High expression of PD-1$^+$/CTLA4$^+$ double-positive cells on TILs in patients with cancer. **A,** Percentage of PD-1$^-$/CTLA4$^-$, PD-1$^+$/CTLA4$^-$, PD-1$^-$/CTLA4$^+$, and PD-1$^+$/CTLA4$^+$ on CD4$^+$ and CD8$^+$ colorectal cancer (CRC; $n = 10$), NSCLC ($n = 14$), RCC ($n = 10$), and melanoma ($n = 10$) TILs isolated from disaggregated tumors. **B,** Representative plot highlighting percentage of PD-1$^-$/CTLA4$^-$, PD-1$^+$/CTLA4$^-$, PD-1$^-$/CTLA4$^+$, and PD-1$^+$/CTLA4$^+$ on CD4$^+$ and CD8$^+$ NSCLC TILs isolated from disaggregated tumors. **C,** Proportion of PD-1$^-$/CTLA4$^-$, PD-1$^+$/CTLA4$^-$, PD-1$^-$/CTLA4$^+$, and PD-1$^+$/CTLA4$^+$ on CD4$^+$ and CD8$^+$ NSCLC TILs isolated from disaggregated tumors represented in **B** that are CD39$^+$. **D,** Analysis of PD-1$^+$/CTLA4$^+$ expression on TILs from 183 tumors across four indications. **E,** PD-1 and CTLA4 expression in coregistered serial sections from NSCLC-Sq sample. Sq, squamous; Ad, adenocarcinoma.

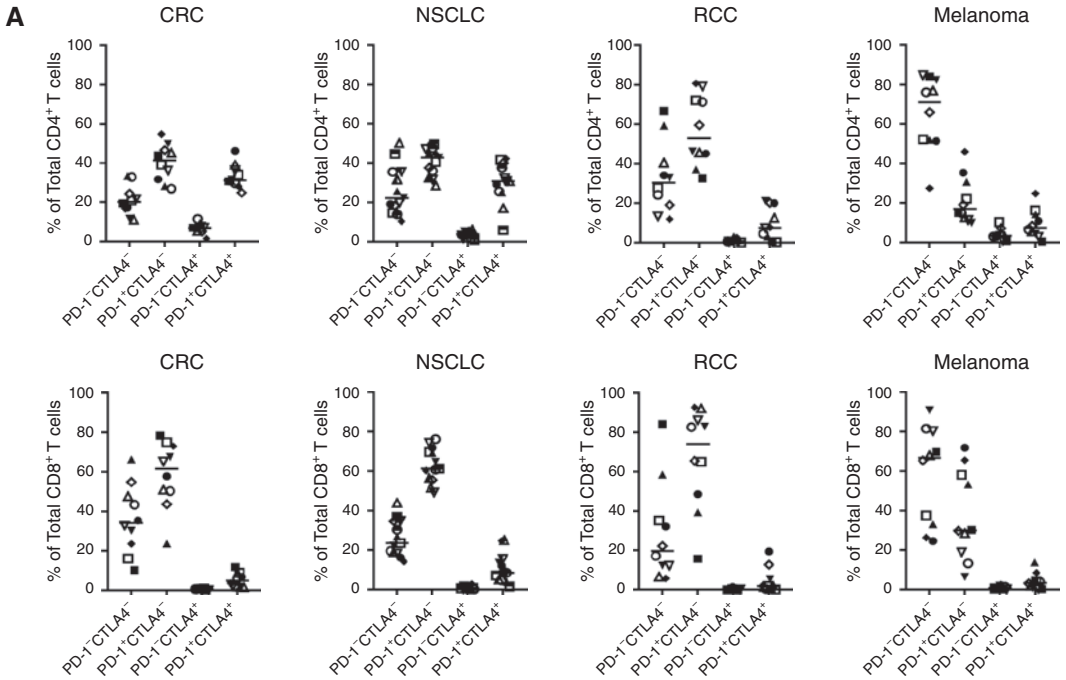

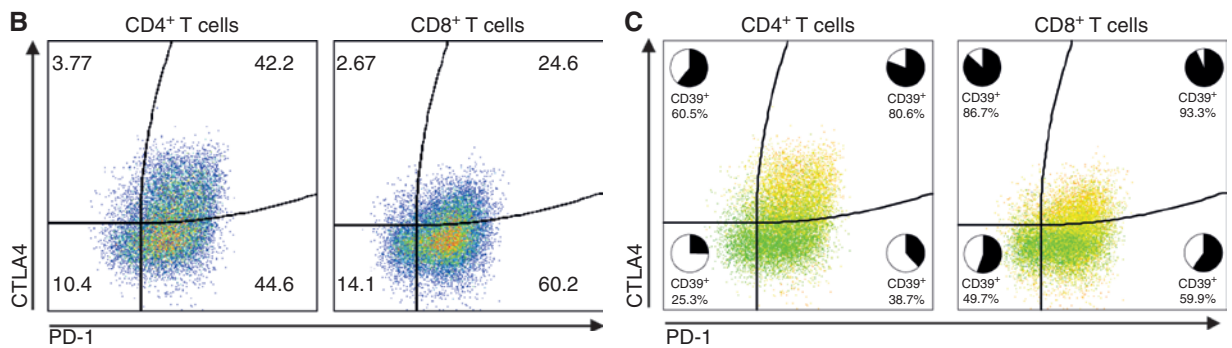

D

	SCCHN	NSCLC-Sq	NSCLC-Ad	UCC
High number of double positives	17%	45%	35%	32%
Low number of double positives	63%	39%	54%	58%
Double positive unlikely/undetected	20%	16%	11%	10%

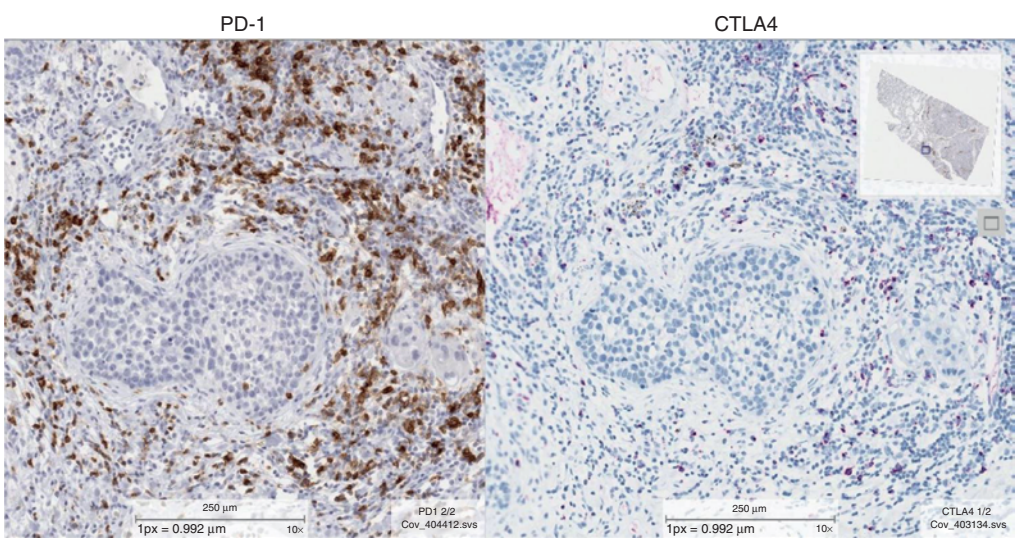

assays. The switch to monovalent targeting of PD-1 as either MEDI5752 or a monovalent PD-1 (mvPD-1) had limited impact (3.5- and 3.8-fold, respectively) on potency when compared with a bivalent anti–PD-1 mAb (Fig. 2A and B). In comparison, monovalent targeting of CTLA4 with either MEDI5752 or a monovalent CTLA4 (mvCTLA4) resulted in a 14.9- and 13.3-fold reduction in potency respectively when compared with a bivalent CTLA4 mAb (Fig. 2C and D). Next, we tested the functional consequence of monovalent targeting of PD-1 in a peripheral blood mononuclear cell (PBMC) assay. In agreement with the two-cell reporter assay, these data showed that valence had little effect on PD-1 inhibition [1.14-fold difference in minimum effective concentration (MEC) required to induce a 2-fold increase in IL2 secretion from PBMC; Fig. 2E and F]. However, valence had a significant impact when targeting CTLA4, with an 8.1-fold increase in the concentration of an mvCTLA4 required to induce this increase in IL2 secretion from PBMC when compared with a bivalent molecule (Fig. 2G and H). These results demonstrate that valence is important for effective functional CTLA4 blockade and that MEDI5752 binding/inhibition of CTLA4 may be significantly weaker on PD-1$^-$ T cells.

MEDI5752 Preferentially Inhibits CTLA4 on PD-1$^+$ Cells

In the case of bispecific antibodies targeting two distinct cell-surface antigens, the relative density of the two receptors has a strong effect on the binding kinetics (42). The bispecific antibody is predisposed to bind first to the more highly expressed receptor as a function of its abundance; hence, the occupancy of the predominant receptor will depend only on the intrinsic binding affinity of the monovalent arm to that receptor. Upon binding of the first arm, the unbound arm is now confined to a limited hemispheric space with a radius equal to the length of the antibody. Consequently, the effective concentration of the less predominant receptor in this constrained volume dramatically increases, and as a result the binding kinetics of the second arm is significantly enhanced. We define the binding mode of the second arm as "cooperative binding" (Fig. 3A). Thus, the occupancy of the less highly expressed receptor is likely to occur at progressively lower concentrations of the bispecific antibody and may exceed the intrinsic affinity of the antibody–antigen interaction by orders of magnitude. The magnitude of this effect appears proportional to the receptor ratio. Given the higher receptor density of PD-1 over CTLA4 on double-positive T cells, the ability of MEDI5752 to preferentially target and saturate CTLA4 on CHO PD-1$^+$CTLA4$^+$ cells, compared with CHO PD-1$^-$CTLA4$^+$ cells expressing only CTLA4, was tested. MEDI5752 saturated the CTLA4 receptor on CHO PD-1$^+$CTLA4$^+$ (10:1) and CHO PD-1$^+$CTLA4$^+$ (40:1) cells at approximately 40- and 500-fold lower concentration, respectively, compared with CHO PD-1$^-$CTLA4$^+$ cells expressing only CTLA4 (Fig. 3B; Supplementary Fig. S9). Next, we tested the functional consequence of cooperative binding of MEDI5752 to PD-1/CTLA4 double-positive cells. To model this, primary human PBMCs were preincubated with or without saturating doses of anti–PD-1, generating model CTLA4 single-positive and PD-1/CTLA4 double-positive cells. Conceptually MEDI5752 will bind to PD-1 preblocked PBMC only via freely available CTLA4; however, on non-preblocked PBMC, MEDI5752 will bind preferentially and facilitate augmented activity. These data showed that cooperative binding reduces the MEC of MEDI5752 required to induce a 3-fold increase in IL2 secretion from anti-CD3 and Staphylococcal Enterotoxin B (SEB)–stimulated PBMC by 93.55-fold (Fig. 3C and D). These results suggest that MEDI5752 can preferentially inhibit CTLA4 on PD-1$^+$ activated versus nonactivated T cells.

MEDI5752 Leads to the Internalization and Degradation of PD-1

The CTLA4 receptor has been reported to rapidly internalize from the plasma membrane in a clathrin- and dynamin-dependent manner driven by the well-characterized YVKM trafficking motif, resulting in only a small fraction of the receptor presented on the cell surface at any given time (20). It was further estimated that more than 80% of cell-surface CTLA4 is internalized within 5 minutes at steady state (24). As such, the internalization properties of MEDI5752 and parental mAbs into CHO PD-1$^+$CTLA4$^+$ (10:1) cells and stimulated primary human CD4$^+$ and CD8$^+$ T cells were interrogated. These data showed that both MEDI5752 and anti-CTLA4 mAb rapidly internalized, whereas anti–PD-1 mAb showed limited internalization (Fig. 4A–E). We next demonstrated that upon concurrent cellular binding and internalization, MEDI5752 induced a dose- and time-dependent downregulation of cell-surface PD-1 in CHO PD-1$^+$CTLA4$^+$ (10:1) cells, promoting more than 90% receptor downregulation after 6 hours of incubation (Supplementary Fig. S10). In contrast, under the same conditions, the parental anti–PD-1 mAb mediated only moderate receptor downregulation (Supplementary Fig. S10). Similarly, cell-surface PD-1 downregulation was observed on both CD4$^+$ and CD8$^+$ T cells after MEDI5752 treatment (Supplementary Fig. S11A–S11D). Removal of MEDI5752 from the culture media led to recovery of cell-surface PD-1 on both CD4$^+$ and CD8$^+$ T cells (Supplementary Fig. S11). Collectively, these data indicate that both MEDI5752 and anti-CTLA4 mAbs efficiently internalized into CHO PD-1$^+$CTLA4$^+$ cells and stimulated CD4$^+$ and CD8$^+$ T cells.

To access the fate of the PD-1 and CTLA4 receptors upon concurrent cellular binding and internalization of MEDI5752, PD-1$^+$SNAP-tag/CTLA4$^+$CLIP-tag double-positive CHO cells were generated. MEDI5752 induced the colocalization of PD-1 and CTLA4 receptors; conversely, parental mAbs resulted in no change in colocalization (Supplementary Fig. S12A and S12B). Furthermore, PD-1 and CTLA4 receptors also colocalize with lysosomes upon MEDI5752 treatment (Supplementary Fig. S12C–S12E). Notably, PD-1$^+$SNAP-tag/CTLA4$^+$CLIP-tag double-positive CHO cells (Fig. 4F–H) and stimulated CD4$^+$ T cells (Fig. 4I) treated with MEDI5752 showed profound degradation of cell-surface PD-1 receptor. None of the treatments altered CTLA4 receptor internalization, with approximately 50% of the receptor internalized within 3 to 5 hours (Fig. 4F–H). Notably, degradation of cell-surface PD-1 was dependent upon concurrent binding to recycling CTLA4, as no degradation of PD-1 was induced when MEDI5752 was incubated with the single-positive CHO PD-1$^+$CTLA4$^-$ cells or when the double-positive CHO PD-1$^+$CTLA4$^+$ (10:1) cells were treated with the parental anti–PD-1 (Supplementary Fig. S13A–S13C). Furthermore, given MEDI5752 levels were maintained after

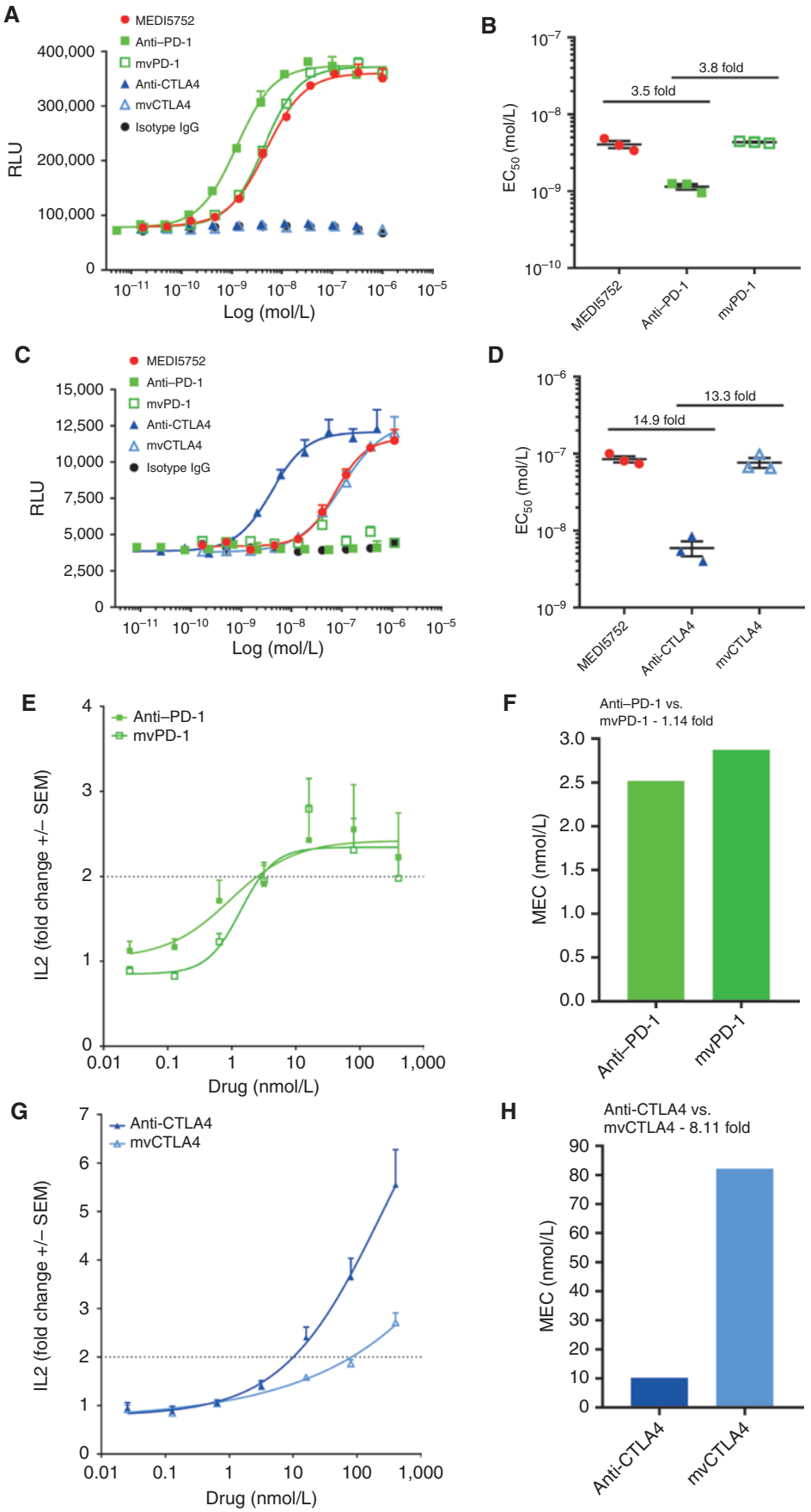

Figure 2. Monovalent targeting reduces the potency of MEDI5752 against CTLA4 but has minimal impact on PD-1. **A** and **B,** Two-cell luciferase reporter assay whereby CHO cells engineered to express PD-L1 and anti-CD3 (OKT3) are cocultured with Jurkat cells engineered to overexpress PD-1. The addition of anti–PD-1 targeting molecules blocks the inhibitory signal mediated via PD-1/PD-L1 interactions facilitating NFAT activation and luciferase gene expression. MEDI5752, anti–PD-1, mvPD-1, and isotype mAbs are added to this coculture, and luciferase expression is detected by Steady-Glo Luciferase assay after 6-hour incubation ($n = 3$, representative example displayed). RLU, relative light units. **B,** Potency was calculated by comparing EC_{50} values of MEDI5752 and mvPD-1 with the EC_{50} value of anti–PD-1. **C** and **D,** Two-cell luciferase reporter assay whereby Raji cells expressing CD80 and CD86 are cocultured with Jurkat cells engineered to overexpress CTLA4 with anti-CD3. The addition of anti-CTLA4 targeting molecules blocks the inhibitory signal mediated via CTLA4/CD80/CD86 interactions, facilitating IL2 activation and luciferase gene expression. MEDI5752, anti-CTLA4, mvCTLA4, and isotype mAbs are added to this coculture, and luciferase expression is detected by Steady-Glo Luciferase assay after 6-hour incubation ($n = 3$, representative example displayed). **D,** Potency was calculated by comparing EC_{50} values of MEDI5752 and mvCTLA4 with the EC_{50} value of anti-CTLA4. **E** and **F,** Human PBMC were stimulated with cytostim in the presence of bivalent anti–PD-1 or mvPD-1 for 72 hours, and IL2 secretion was measured by ELISA ($n = 9$, independent donors). **G** and **H,** Human PBMCs were stimulated with cytostim plus LPS in the presence of bivalent anti-CTLA4 or mvCTLA4 for 72 hours, and IL2 secretion was measured by ELISA ($n = 9$, independent donors). **F** and **H,** The MEC required to induce a 2-fold increase in IL2 secretion from baseline was calculated.

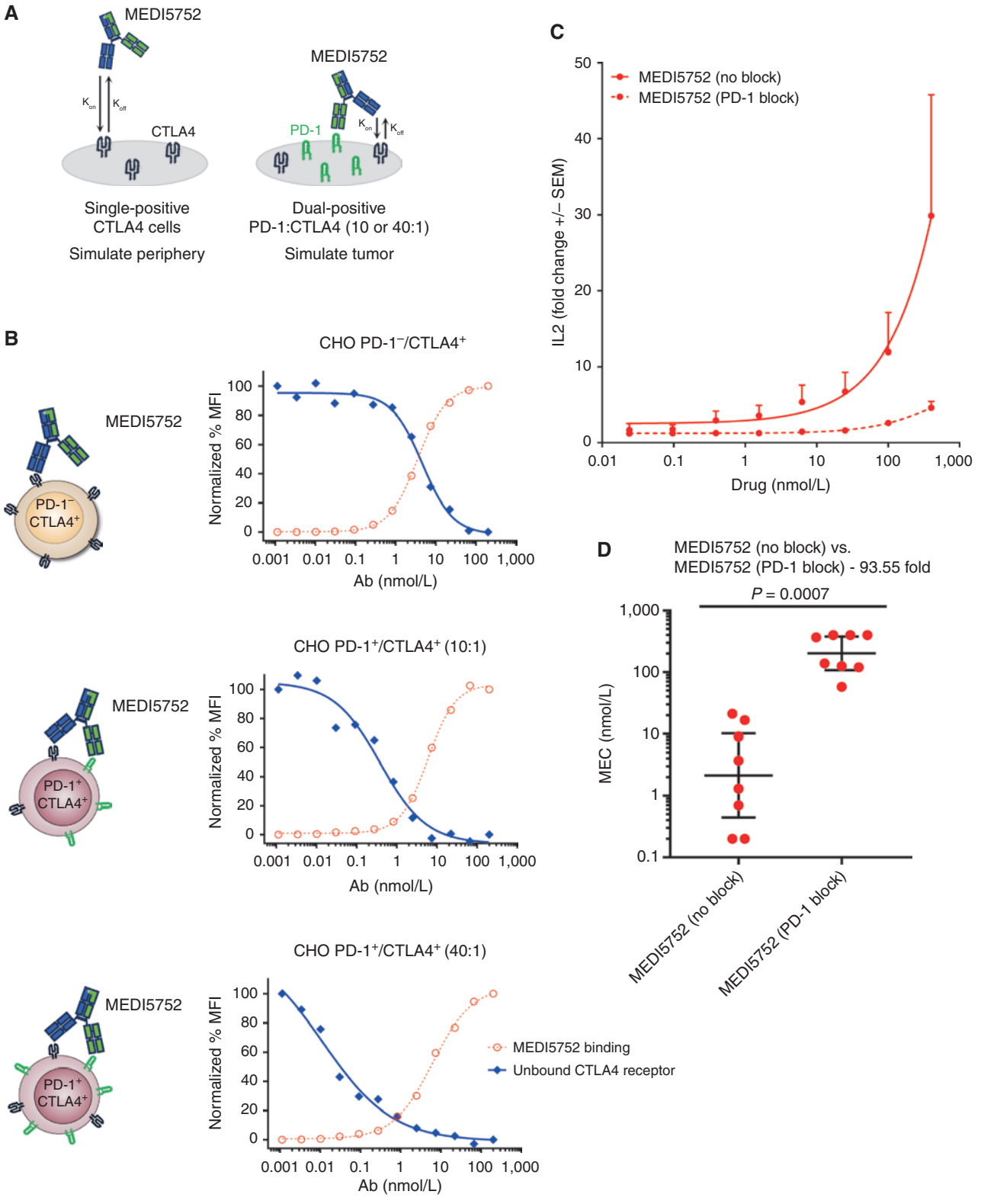

Figure 3. MEDI5752 preferentially targets CTLA4 on double-positive versus single-positive cells. **A,** Diagram representing the binding profile of MEDI5752 to either PD-1⁻/CTLA4⁺ single-positive cells simulating the periphery or PD-1⁺/CTLA4⁺ double-positive cells simulating the tumor. **B,** CHO cell receptor occupancy assay where MEDI5752 was incubated on either PD-1⁻/CTLA4⁺ single-positive or PD-1⁺/CTLA4⁺ double-positive CHO cells and MEDI5752 binding was assessed by flow cytometry. **C** and **D,** Human PBMC were stimulated with anti-CD3 and SEB in the presence of MEDI5752 with or without anti–PD-1 preblock for 72 hours, and IL2 secretion was measured by ELISA ($n = 8$, independent donors). **D,** The MEC required to induce a 3-fold increase in IL2 secretion from baseline was calculated. MFI, mean fluorescence intensity.

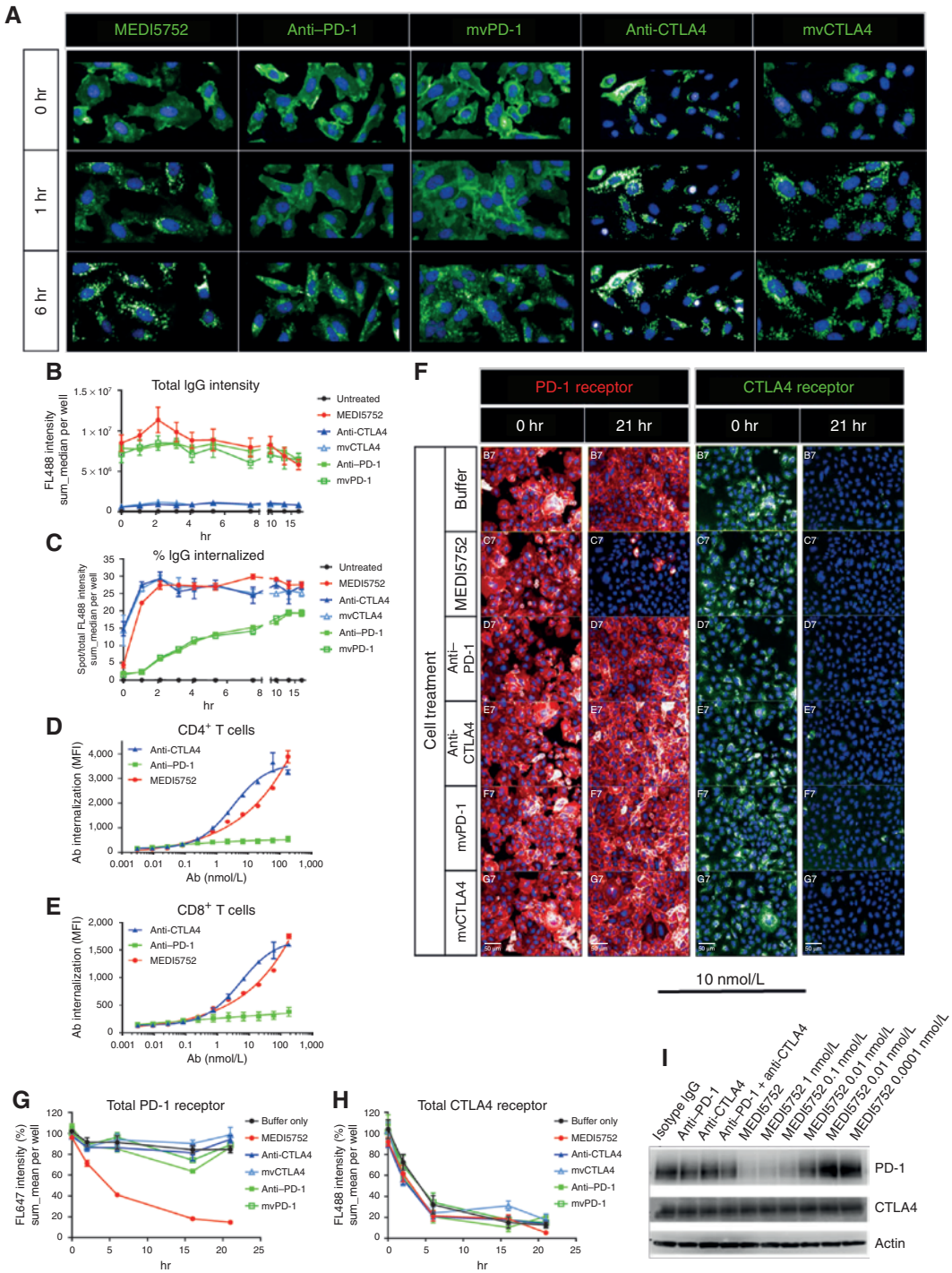

Figure 4. MEDI5752 leads to the internalization and degradation of PD-1. **A–C,** PD-1$^+$/CTLA4$^+$ double-positive CHO cells were pretreated with AF488-labeled MEDI5752, anti–PD-1, mvPD-1, anti-CTLA4, or mvCTLA4 mAbs at 4°C for 30 minutes. After washing to remove excess antibody, cells were incubated at 37°C to initiate internalization and imaged on Opera using 20× objective. Columbus software was used for image analysis. **B,** Total antibody binding was quantified as FL488 sum intensity mean per well. **C,** Antibody internalization was measured as intracellular spot FL488 sum intensity mean per well and divided by total antibody intensity to determine % antibody internalized ($n = 3$, independent experiments). **D** and **E,** Internalization of MEDI5752 and parental mAbs into CD4$^+$ and CD8$^+$ T cells stimulated with anti-CD3 and anti-CD28 mAbs. Internalization was determined by conjugation of the test and control article mAbs with a pH-reactive dye that fluorescence brightly only after internalization and trafficking into acidic intracellular compartments. **F,** PD-1$^+$SNAP-tag/CTLA4$^+$CLIP-tag double-positive CHO cells were prelabeled with SNAP-Cell 647 and CLIP-Cell 505. Cells were treated with MEDI5752, anti–PD-1, anti-CTLA4, mvPD-1, or mvCTLA4 mAbs and imaged over live time course at 37°C. **G** and **H,** PD-1 (**G**) and CTLA4 (**H**) receptor was quantified as FL647 (PD-1) or FL488 (CTLA4) sum intensity mean per well ($n = 3$, independent experiments). **I,** Human CD4$^+$ T cells were stimulated with Phytohaemagglutinin in the presence of MEDI5752, anti–PD-1, anti-CTLA4, or a combination of anti–PD-1 and anti-CTLA4 mAbs for 24 hours. PD-1 and CTLA4 protein expression was analyzed by Western blot ($n = 4$, independent donors, representative blot showed). Each point represents the mean values of duplicate wells, and the ±SEM is represented by error bars.

treatment (Fig. 4B), it is likely MEDI5752 is not degraded, unlike PD-1. We next tested whether these findings were phenocopied on human NSCLC TILs treated with MEDI5752. Similarly, MEDI5752 induced profound downregulation of PD-1 in CD4$^+$ FOXP3$^-$ T cells compared with an isotype mAb control or a combination of anti–PD-1 and anti-CTLA4 mAbs (Supplementary Fig. S14A–S14C).

MEDI5752 Preferentially Targets CTLA4 on Double-Positive Cells Compared with mAb Combination

Next, the ability of MEDI5752 to preferentially target and saturate the CTLA4 receptor on CHO PD-1$^+$CTLA4$^+$ cells was assessed (Fig. 5A and B). MEDI5752 saturated the CTLA4 receptor on CHO PD-1$^+$CTLA4$^+$ (10:1) and CHO PD-1$^+$CTLA4$^+$ (40:1) cells at approximately 10- and 250-fold lower concentration, respectively, compared with anti-CTLA4 mAb coadministered with anti–PD-1 mAb (Fig. 5B; Supplementary Fig. S9). Furthermore, there was no difference in the capacity of MEDI5752 to saturate the PD-1 receptor when compared with anti-CTLA4 mAb coadministered with anti–PD-1 mAb (Fig. 5B; Supplementary Fig. S9). Next, we tested the functional consequence of cooperative binding of MEDI5752 on anti-CD3/SEB stimulated PBMC. These data showed that cooperative binding of MEDI5752 reduces the MEC required to induce a 3-fold increase in IL2 secretion from PBMC when compared with a combination of anti–PD-1 mAb with either bivalent anti-CTLA4 or mvCTLA4 mAbs by 42.33- and 96.35-fold, respectively (Fig. 5C and D). These results suggest that MEDI5752 may provide enhanced efficacy over a combination of mAbs targeting PD-1 and CTLA4.

As CTLA4 can modulate T-cell activation both intrinsically and extrinsically via expression on Treg, we determined the activity of MEDI5752 in an *in vitro* assay where primary Treg were cocultured with allogeneic CD3$^+$ T cells and allogeneic PBMC (depleted of CD3$^+$ cells) to reconstruct a three-way mixed lymphocyte reaction where relevant costimulatory molecules are present. Our data demonstrate that the combination of inhibitory PD-1 and CTLA4 mAbs can overcome Treg-mediated suppression of Teff cells. Treatment with MEDI5752 led to significantly greater secretion of IFNγ (1.9–3.3-fold at Treg:Teff ratios of 1:4 and 1:8) when compared with a combination of parental mAbs (Fig. 5E). The effect of PD-1/CTLA4 blockade with conventional mAbs and with MEDI5752 on IFNγ production by both CD4$^+$ and CD8$^+$ T cells was confirmed by flow cytometry (Fig. 5F and G). Taken together, these data demonstrate that MEDI5752 has increased activity when compared with a combination of PD-1/CTLA4 mAbs in the context of T-cell activation and overcoming Treg-mediated suppression.

MEDI5752 Preferentially Localizes to the Tumor and Inhibits Tumor Growth *In Vivo*

Due to the lack of cross-reactivity of MEDI5752 with murine PD-1 and CTLA4, a novel transgenic mouse model expressing human PD-1 and human CTLA4 on immune cells (C57BL/6N-*Pdcd1*$^{tm1(huPDCD1\text{-}ICP11)Geno}$ *Ctla4*$^{tm1(huCTLA4\text{-}ICP13)Geno}$; hereafter designated PD-1^{huKI}/CTLA4^{huKI}) was used to study the *in vivo* activity of MEDI5752. Biodistribution studies using radiolabeled molecules in mice bearing MCA205 tumors revealed that significantly higher levels of MEDI5752 localized to the tumor when compared with a conventional anti-CTLA4 or isotype mAb (Fig. 6A–D). For MEDI5752, we confirmed this tumor localization was a consequence of target binding, as no increase in tumor localization was observed in mice bearing wild-type PD-1/CTLA4 receptors. We observed no significant difference in tumor localization when comparing MEDI5752 with a conventional anti–PD-1 mAb. These data suggest that the biodistribution of the antibodies was dependent on PD-1 expression and binding. Moreover, this significant increase in tumor localization of MEDI5752 when compared with a CTLA4 mAb demonstrates the potential for enhanced blockade of the receptor in the TME. Furthermore, we showed strong, dose-dependent antitumor activity of MEDI5752 in this model, achieving complete tumor clearance in more than 60% of mice when administered at 10 mg/kg (Fig. 6E). When compared with monotherapy with anti–PD-1 or anti-CTLA4 mAb only, a single dose of MEDI5752, but not a combination of parental mAbs, led to increased survival (Fig. 6F). Moreover, in NOD/SCID gamma (NSG) mice infused with human viral–specific T cells bearing human viral peptide–transduced OE21 tumors, treatment with MEDI5752 inhibited tumor growth to a greater extent than a combination of parental mAbs (Fig. 6G). These data provide evidence that MEDI5752 can preferentially localize to the tumor when compared with a CTLA4 mAb, and provide improved efficacy when compared with conventional PD-1/CTLA4 mAbs.

MEDI5752 Has Demonstrated Activity in Advanced Solid Tumors

MEDI5752 is being evaluated in an ongoing first-time-in-human study in advanced solid tumors (NCT03530397). Here, we present preliminary data as illustrative evidence of clinical activity with a partial response with 60% tumor reduction in a 61-year-old patient with gastric adenocarcinoma who had failed five prior lines of chemotherapy (Fig. 7A) and a partial response with 68% tumor reduction in a 51-year-old patient with treatment-naïve clear cell carcinoma of the kidney (Fig. 7B). Both remain progression-free at 80 and 24 weeks, respectively, with manageable toxicities.

Figure 5. MEDI5752 preferentially targets CTLA4 on double-positive cells compared with a combination of anti–PD-1 and anti-CTLA4 mAbs and shows superior activity to a combination of anti–PD-1 and anti-CTLA4 mAbs in an *in vitro* Treg suppression assay. **A,** Diagram representing the binding profile of MEDI5752 or a combination of anti–PD-1 and anti-CTLA4 mAbs to PD-1$^+$/CTLA4$^+$ double-positive cells. **B,** CHO cell receptor occupancy assay where MEDI5752 or a combination of anti–PD-1 and anti-CTLA4 mAbs were incubated on PD-1$^+$/CTLA4$^+$ double-positive CHO cells and drug binding was assessed by flow cytometry ($n = 3$, representative of three experiments). **C** and **D,** Human PBMC were stimulated with anti-CD3 and SEB in the presence of MEDI5752, anti-CTLA4 with fixed dose anti–PD-1, or mvCTLA4 with fixed dose anti–PD-1 for 72 hours, and IL2 secretion was measured by ELISA ($n = 8$, independent donors). **D,** The MEC required to induce a 3-fold increase in IL2 secretion from baseline was calculated. **E–G,** Human Tregs were cocultured with allogeneic CD3$^+$ T cells and allogeneic PBMC (depleted of CD3$^+$ cells) and stimulated with anti-CD3 with either MEDI5752, anti–PD-1, anti-CTLA4, a combination of anti–PD-1 and anti-CTLA4, or isotype mAbs for 96 hours, and total IFNγ secretion and IFNγ derived from CD4$^+$ and CD8$^+$ T cells respectively were measured by ELISA and intracellular flow cytometry ($n = 3$, independent donors, representative of three experiments).

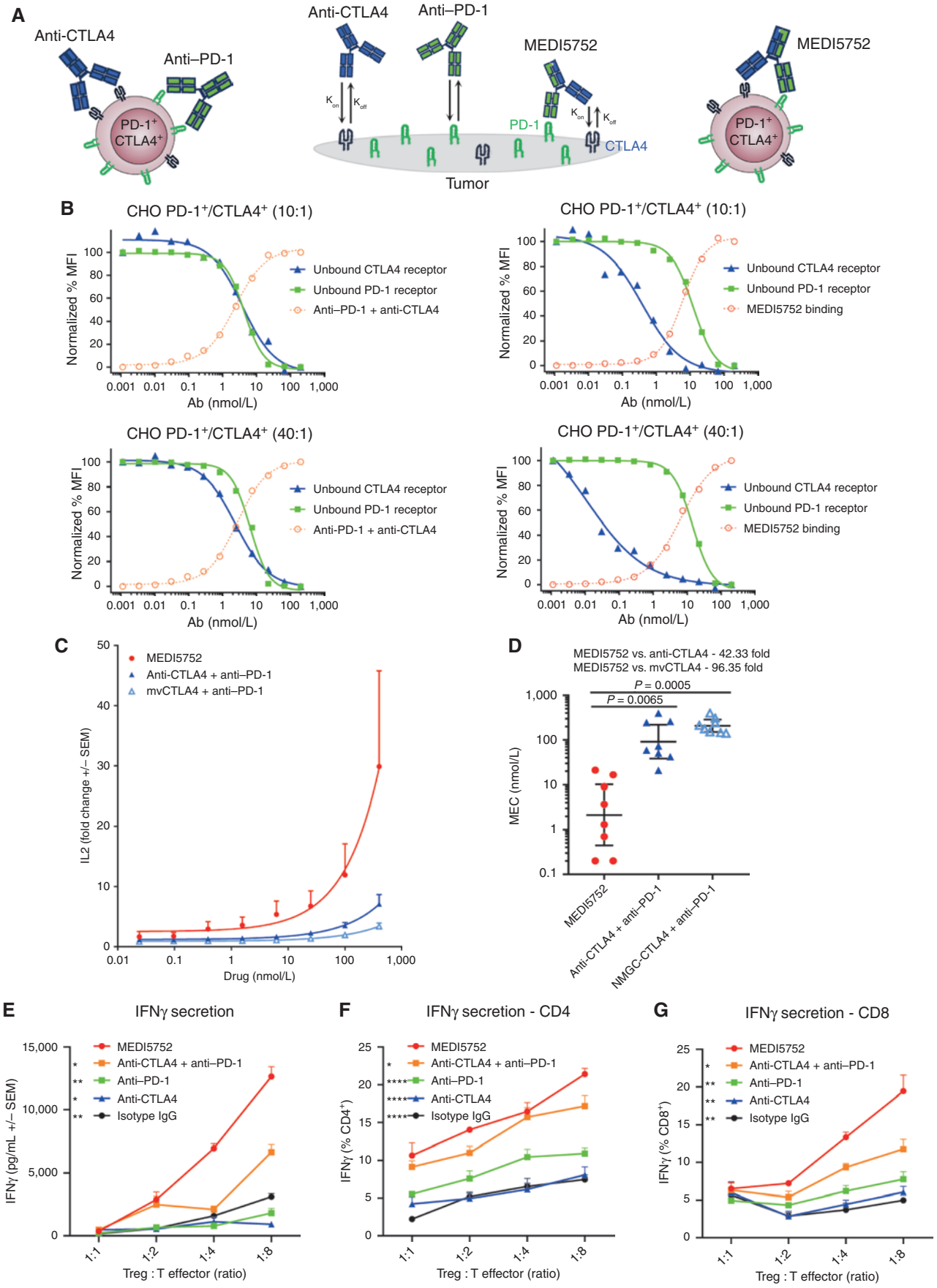

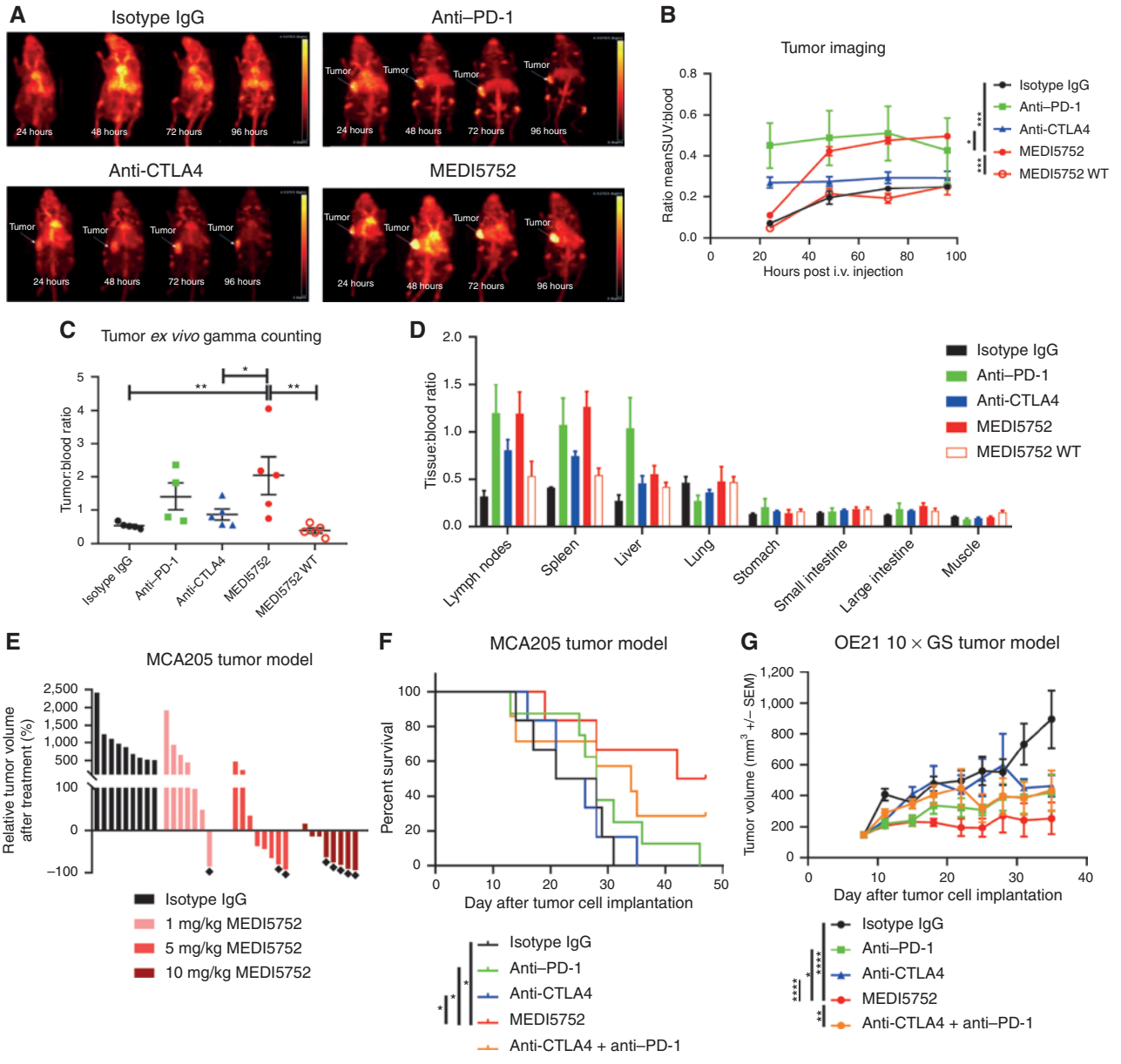

Figure 6. MEDI5752 inhibits tumor growth *in vivo* and preferentially localizes to the tumor. **A–F,** Transgenic PD-1^{huKI}/CTLA4^{huKI} mice (or C57BL/6 wild-type control mice when indicated as WT) were subcutaneously implanted with MCA205 tumors. **A** and **B,** On day 15 after implantation, ^{89}Zr-labeled MEDI5752, anti–PD-1, anti-CTLA4, and isotype mAbs were i.v. dosed (5 mice per group), and PET imaging was performed at 24, 48, 72, and 96 hours after dosing. Tracer uptake in the region of interest was normalized to blood tracer levels and plotted as meanSUV:blood ratio. Statistical significance was calculated using a mixed-effects model with Dunnett multiple comparisons test. **C,** Ninety-six hours after dosing, animals were sacrificed, and tumors were collected. Tracer uptake was quantified *ex vivo* by gamma counting and expressed as the ratio of tumor to blood tracer levels. Statistical significance was calculated using a one-way ANOVA with Dunnett multiple comparison test. **D,** Ninety-six hours after dosing, animals were sacrificed and tissues were collected. Tracer uptake was quantified *ex vivo* by gamma counting and expressed as the ratio of tissue to blood tracer levels. **E** and **F,** For assessment of antitumor activity, mice were i.v. injected 5 or 6 days after tumor implantation with 10 mg/kg anti-CD20 antibody to deplete B cells. **E,** Mice were then i.p. injected with MEDI5752 or 10 mg/kg isotype mAb on days 7 and 11 after tumor implantation, and the relative tumor volume at day 19 after tumor implantation was calculated by dividing the difference in tumor volumes at days 19 and 7 by the tumor volume at day 19. Mice that had complete responses are marked with a diamond (8–10 mice per group, data representative of 2 independent experiments). **F,** Mice were i.p. injected on day 11 after tumor implantation with 5 mg/kg MEDI5752, 5 mg/kg anti–PD-1, 5 mg/kg anti-CTLA4, a combination of 5 mg/kg anti–PD-1 and 5 mg/kg anti-CTLA4, or isotype mAb, and survival was monitored over time (6–8 mice per group). Statistical significance was calculated using a log-rank test **G,** NSG mice were s.c. implanted with viral peptide-transduced OE21 tumor cells. On day 7 after tumor implantation, mice were i.v. injected with *in vitro* viral peptide–stimulated PBMC. 10 mg/kg MEDI5752, 10 mg/kg anti–PD-1, 10 mg/kg anti-CTLA4, a combination of 10 mg/kg anti–PD-1 and 10 mg/kg anti-CTLA4, or isotype mAbs were then i.p. injected on days 9, 11, 14, and 17 after tumor implantation, and tumor growth was monitored over time (10 mice per group, data representative of 2 independent experiments). Statistical significance was calculated using a mixed-effects model with Dunnett multiple comparisons test. $P > 0.05$; *, $P < 0.05$; **, $P < 0.01$; ***, $P < 0.001$; ****, $P < 0.0001$.

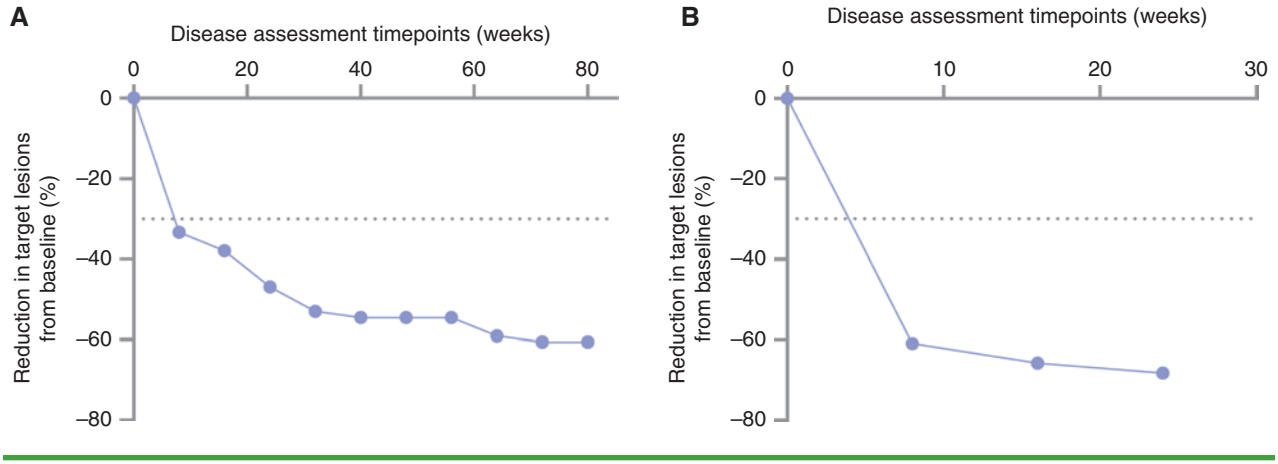

Figure 7. Tumor response induced by MEDI5752 and measured by a reduction in target lesion size compared with baseline (**A**) in a patient with gastric adenocarcinoma and (**B**) in a patient with clear cell carcinoma of the kidney.

DISCUSSION

Recent published studies demonstrate the innovation being applied to engineer improved antibody-based cancer immunotherapies as the field moves beyond conventional mAb (43–45). In this study, we describe the characterization of MEDI5752, a novel monovalent bispecific antibody designed to provide modulated CTLA4 engagement, favoring binding/inhibition on activated T cells expressing PD-1.

The contribution of Fc-mediated depletion of Treg by anti-CTLA4 mAbs remains contentious without clear evidence that this occurs in the clinic with ipilimumab or tremelimumab (46, 47). Our data demonstrate that CTLA4 expression is also enriched on PD-1$^+$ CD4$^+$ and CD8$^+$ TILs and that on these cells PD-1 is expressed in excess *cf.* CTLA4. Moreover, we show that these PD-1$^+$CTLA4$^+$ TILs also express CD39, a marker of antigen experience and exhaustion (39, 48), suggesting that these cells may be relevant contributory effectors of CTLA4-mediated antitumor activity. Moreover, this pattern of coexpression for CTLA4 and PD-1 underscores the design of the Fc domain of MEDI5752 which incorporates three mutations to reduce effector function (41), thereby preventing depletion of effector populations critical for response.

CTLA4 can also be expressed on the surface of naïve T cells following signaling through the TCR and serves to attenuate T-cell activation. Clinical studies have demonstrated that CTLA4 blockade, presumably in secondary lymphoid organs, can increase the diversity of the peripheral TCR repertoire which is associated with both response and the onset of irAEs (37, 49). Interestingly, the stability of T-cell clonotypes present prior to the initiation of anti-CTLA4 mAb therapy has also been associated with improved survival in patients with cancer (37). It remains unclear how this peripheral change in TCR diversity/stability is influenced by CTLA4 blockade specifically on naïve T cells and/or on Treg cells, and moreover how this inhibition in the secondary lymphoid organs may contribute to antitumor activity. Furthermore, recent studies have demonstrated a confluence of the PD-1 and CTLA4 pathways with the identification that the reinvigoration of TILs following PD-1 blockade is dependent on CD28 costimulation (12, 13). These data suggest that concurrent blockade of the PD-1 and CTLA4 pathways on TILs may ultimately be needed to drive an optimal antitumor response. Consistent with this, tumor resident/infiltrating dendritic cells have been shown to be critical for supporting an inflamed TME (50) and for response to ICB (51). Importantly, several preclinical studies have also demonstrated that local blockade of CTLA4 within the tumor, and not the periphery, can facilitate immune-mediated tumor regressions (28–36). Taken together, these data support the hypothesis that directing CTLA4 inhibition to the TME may be sufficient to engender effective antitumor immune responses. In the TME, CTLA4 can function through the intrinsic pathway, directly affecting the cell expressing CTLA4. Alternatively, CTLA4 can function through the extrinsic pathway, indirectly affecting effector cell function via competition for/sequestration of available costimulatory ligands (21). Indeed, previous studies have demonstrated that inhibition of CTLA4 was required on both effector and regulatory compartments for maximal antitumor activity (18). We show that MEDI5752 can saturate CTLA4 on PD-1$^+$ cells at orders of magnitude lower concentrations than required to saturate CTLA4 on PD-1$^-$ cells. Moreover, our data demonstrate that monovalent targeting of CTLA4 with either MEDI5752 or an mvCTLA4 is significantly less potent than bivalent targeting with a parental anti-CTLA4 mAb. In contrast, the switch to monovalent targeting of PD-1 has limited effect on potency. Together, these data demonstrate the capacity of MEDI5752 to preferentially inhibit CTLA4 on activated T cells (expressing PD-1) with significantly reduced activity on PD-1$^-$ T-cell populations. We hypothesize that these binding characteristics have the potential to provide enhanced CTLA4 blockade that can be achieved clinically with dual ICB.

Clinical data demonstrate a clear dose response for both efficacy and toxicity with CTLA4 inhibition (7, 8). However, our *in vitro* data demonstrate that conventional mAbs are far less able to saturate CTLA4 on primary T cells when compared with PD-1. We hypothesized this may be due to the rapid internalization and recycling kinetics associated with CTLA4, resulting in only a small fraction of the receptor presented on the cell surface at any given time (20, 24).

MEDI5752 leverages cross-arm avidity binding (where one of the fragment antigen-binding domains acts as an anchor for the other) to take advantage of both the more stable surface expression of PD-1 and the elevated cell-surface density of PD-1 versus CTLA4. Our data demonstrate enhanced saturation of CTLA4 with the PD-1/CTLA4 bispecific when compared with equimolar concentrations of a conventional mAb targeting CTLA4 and are consistent with recently reported data demonstrating the capacity of bispecific antibodies to promote improved target selectivity by cross-arm avidity binding to two antigens on the surface of the same cell (52–58). Moreover, we found that tethering PD-1 to CTLA4 also leads to the internalization and subsequent degradation of PD-1, providing a novel mechanism of action that is distinct from other mAbs targeting this axis. In the present study, we focused our observations on functional responses following treatment and did not assess changes in proximal signaling pathways. It is interesting to speculate that the degradation of PD-1 observed with MEDI5752 could potentially influence the dynamics of intracellular signaling when compared with conventional anti–PD-1 mAbs.

Supporting our *in vitro* observations, we further show that MEDI5752 preferentially localizes to the tumor when compared with a conventional anti-CTLA4 mAb and also provides improved efficacy in preclinical models when compared with a combination of PD-1 and CTLA4 mAbs that share the same specificities and intrinsic affinities. Although the biodistribution of MEDI5752 in the periphery was generally comparable to that of a conventional anti-CTLA4 mAb, we have demonstrated that CTLA4 inhibition is significantly reduced in the case of monovalent binding (on PD-1$^-$ T cells or vs. a conventional bivalent anti-CTLA4 mAb). Moreover, we present preliminary evidence illustrating the clinical activity of MEDI5752 from an ongoing first-time-in-human study of MEDI5752 in advanced solid tumors. These clinical data represent anecdotal evidence and should therefore be interpreted with caution. A multicenter phase I study is ongoing across a range of solid tumor types (NCT03530397) to examine the safety, pharmacokinetic/pharmacodynamic relationship, and efficacy of MEDI5752.

Modulating the inhibition of CTLA4 to favor blockade on PD-1$^+$ T cells using a monovalent bispecific may provide a tractable method for directing CTLA4 blockade to antigen-experienced T cells. This approach may facilitate enhanced CTLA4 blockade beyond that achievable with current PD-1/PD-L1 and CTLA4 mAb combinations and has the potential to improve responses in tumors sensitive to dual checkpoint blockade and also open opportunities in tumor types where suboptimal exposures have prevented clinically meaningful activity.

METHODS

Antibody Construction

MEDI5752 was constructed on the backbone of the DuetMab molecule essentially as described (40). Briefly, the variable heavy (VH) and variable light (VL) genes of the anti-CTLA4 tremelimumab were inserted into a human gamma-1 constant heavy chain carrying the "Knob" mutation and an engineered constant Lambda light chain, respectively. The VH and VL genes of an in-house anti–PD-1 mAb were inserted into a human gamma-1 constant heavy chain carrying the "Hole" mutations and a constant Kappa light chain, respectively. Collectively, the frameworks and complementarity determining regions for the PD-1 and CTLA4 mAbs were identical to those incorporated in MEDI5752. The Fc domain was further engineered to carry the triple mutations (L234F, L235E, and P331S) designed to reduce Fc-mediated immune effector functions (41). For the construction of mvCTLA4 and mvPD-1 antibodies, the VH and VL genes of the anti-CTLA4 and anti–PD-1 mAbs were paired with the VH and VL genes of an isotype control to form heterodimer mvCTLA4 and mvPD-1 antibodies, respectively.

Concurrent Biochemical Binding

Concurrent binding studies to recombinant human and cynomolgus monkey PD-1 and CTLA4 proteins were measured by biolayer interferometry on an Octet384 instrument (ForteBio). Biotinylated human PD-1 protein at 5 μg/mL in assay buffer [PBS pH 7.2, 3 mg/mL BSA, and 0.05% (v/v) Tween 20] was captured on streptavidin (SA) biosensors (ForteBio). Cynomolgus monkey PD-1–FLAG/10 HIS protein at 5 μg/mL in assay buffer was captured on anti-Penta HIS (HIS1K) biosensors (ForteBio). Following a washing step to remove any unbound protein, the respective loaded biosensors were subjected to successive association and dissociation interactions, first with 5 μg/mL of MEDI5752 and then with human or cynomolgus monkey CTLA4 antigen at 5 μg/mL. Association and dissociation curves were calculated from a nonlinear fit of the data using the Octet384 software v.9.0.

Concurrent Binding to Cell-Surface Receptors

To determine concurrent binding of PD-1 and CTLA4 receptors by cell-bound MEDI5752, CHO PD-1$^+$CTLA4$^-$ and CHO PD-1$^+$CTLA4$^+$ (10:1) were incubated with 3-fold serial dilutions of MEDI5752 or parental anti–PD-1 mAb starting at a concentration of 6.7 nmol/L for 30 minutes at 4°C. After washing with FACS buffer, cell-bound antibodies were detected by phycoerythrin (PE)-conjugated goat anti-human Fcγ antibody (Jackson ImmunoResearch), and free antigen-binding arms were detected by biotinylated soluble CTLA4 and PD-1 proteins at 5 nmol/L followed by SA–allophycocyanin (BioLegend). After incubation for 30 minutes at 4°C, cells were washed and fixed with 4% paraformaldehyde (PFA) for 10 minutes. Fluorescence detection of cell-bound IgG (PE) and monovalent binding to soluble antigens (allophycocyanin) was determined using an LSRII flow cytometer (BD Biosciences). Data analysis was performed using the FlowJo software, and the mean fluorescence intensity (MFI) was used to determine binding intensity. Based on physical properties (height, width, and density), only single cells were gated for analysis. All data analyses were performed using GraphPad Prism version 7.02 for Windows (GraphPad Software).

Cellular Cooperative Binding Analyses

Cooperative binding assays were performed by flow cytometry using a MACSQuant VYB (Miltenyi Biotec) instrument. To allow unbound receptor detection, parental anti–PD-1 and anti-CTLA4 mAbs were labeled with Alexa Fluor 647 and Alexa Fluor 488 labeling kits (Invitrogen), respectively, according to the manufacturer's instructions. Antibody concentration and fluorochrome to protein (F:P) ratio was calculated by a ND-1000 spectrophotometer (NanoDrop). Antibody cell-binding and receptor occupancy were determined simultaneously. CHO PD-1$^-$CTLA4$^+$, CHO PD-1$^+$CTLA4$^+$ (10:1), and CHO PD-1$^+$CTLA4$^+$ (40:1) cell lines at 2×10^5 viable cells/well were first washed with ice-cold assay buffer (PBS pH 7.2 with 1% FBS) and then incubated with 3-fold serial dilutions of unconjugated antibodies or a combination of unconjugated anti–PD-1 + anti-CTLA4 mAbs. After incubation for 30 minutes at 4°C, cells were washed and fixed with 4% PFA for 5 minutes. Unbound PD-1 receptor was detected with 15 μg/mL of anti–PD-1-Alexa Fluor 647 conjugate, whereas unbound CTLA4 receptor was detected using 15 μg/mL of anti-CTLA4-Alexa Fluor 488 conjugate. For the detection of cell-bound unconjugated

antibodies, BV421-conjugated mouse anti-human IgG Fcγ (BioLegend) was used. The amount of antibodies bound to the cell surface was determined using MACSQuantify software. Data analysis was performed using the FlowJo software, and the MFI was used to determine binding intensity. Based on physical properties (height, width, and density), only single cells were gated for analysis. Bound antibody signal was normalized between maximal MFI signal at the highest concentration tested and signal in a no-antibody control. Unbound receptor signal was normalized between the maximal signal in a no-antibody control and signal obtained with 15 μg/mL of labeled IgGs, which was far above the concentration required to saturate estimated cell-surface antigen levels. All data analyses were performed using GraphPad Prism version 7.02 for Windows (GraphPad Software).

Human Treg Suppression Assay

$CD4^+$ $CD25^+$ $CD127^{low}$ human Treg (Donor 1) were isolated (StemCell Technologies) and 1×10^6 cells were expanded for 6 days in differentiation medium [X-Vivo 15 media (Lonza) supplemented with 5% human serum, 1% penicillin–streptomycin, 5×10^5 CD3/CD28 activation beads (Thermo Fisher Scientific), and 100 IU IL2 (Corning)]. At day 6, Treg were harvested, washed with PBS, and rested for 24 hours in X-Vivo 15 media supplemented with 5% human serum and 1% penicillin–streptomycin. At day 7, allogeneic responder T cells (Donor 2) and T cell–depleted PBMC (Donor 3) were isolated (Stemcell). Treg and responder T cells were stained with Cell Trace Violet and carboxyfluorescein succinimidyl ester proliferation dyes respectively (Thermo Fisher Scientific) and resuspended in assay medium (RPMI-1640 Glutamax I culture media supplemented with 10% FBS and 1% penicillin–streptomycin) to 1×10^6 cells/mL. T cell–depleted PBMC were resuspended in assay medium to 2×10^6 cells/mL. 5×10^4 responder T cells and 1×10^5 T cell–depleted PBMC were added to each well, and 5×10^4 Treg were titrated 1 in 2 across a 96-well round-bottomed tissue culture–treated plate. 1 μmol/L of MEDI5752, anti–PD-1, anti-CTLA4, a combination of anti–PD-1 and anti-CTLA4, or an isotype mAbs were added to cultures with 1 μg/mL anti-CD3 antibody (clone OKT3, Thermo Fisher Scientific). Cell cultures were incubated at 37°C with 5% CO_2 for 4 days. At day 3, Golgi stop and Golgi plug (BD Biosciences) were added to each culture well, and cells and supernatants were harvested at day 4. IFNγ secretion was evaluated by ELISA (R&D Systems), and intracellular IFNγ secretion was evaluated by flow cytometry.

IgG Drug Internalization by High Content Imaging

Antibodies were first conjugated with the Alexa Fluor 488 Protein Labeling Kit (Invitrogen) according to the manufacturer's instructions. Retention of binding of labeled IgG was confirmed by flow cytometry on target expressing cells and compared with an unlabeled IgG using an Alexa Fluor 647–labeled anti-human IgG antibody.

$PD\text{-}1^+$/$CTLA4^+$ double-positive CHO cells were labeled with Cell Tracker according to the manufacturer's instructions. Briefly, cells in flask were incubated with 2 μmol/L Cell Tracker red CMTPX (Molecular Probes) in serum-free media. After 45 minutes at 37°C, stain was removed and replaced with complete media. Cells were incubated for another 30 minutes at 37°C. After washing, cells were plated at 2×10^4 per well in a 96-well plate and were incubated overnight at 37°C. Next day, cells were prelabeled with 2 μg/mL Hoechst 33342 (Invitrogen) and 40 nmol/L AF488-labeled IgG for 30 minutes at 4°C to avoid internalization. After washing to remove excess antibody, cells were incubated at 37°C to initiate internalization and imaged.

Antibody Internalization Analyses

Antibody internalization properties were determined by flow cytometry using pH-reactive dye antibody conjugates that fluoresce brightly only after internalization and trafficking into acidic intracellular compartments. Antibodies were first conjugated with thiol reactive dye pHAb kit (Promega) according to the manufacturer's instructions and then used in serial dilution starting at 180 nmol/L. All antibody dilutions were done in the appropriate culture media for the specified target cells. Cells were added as indicated at 5×10^4 cells/well and 1×10^4 cells/well for CHO and primary $CD3^+$ T cells, respectively, followed by culture at 37°C with 5% CO_2 for time intervals of 3 hours for CHO cells and 4 hours for primary $CD3^+$ T cells. For Time 0 control (background), cells were incubated at 4°C for 30 minutes. After incubation, cells were washed with FACS buffer to remove excess antibody, and CHO cells were fixed in 4% PFA prior to analysis using an LSR II flow cytometer (BD Biosciences). Primary $CD3^+$ T cells were additionally costained with anti-CD4 (clone RPA-T4, BioLegend) and anti-CD8 (clone RPA-T8, BioLegend) antibodies, and a viability dye (4′,6-diamidino-2-phenylindole or propidium iodide, Sigma) was used to discern each live population. Cells were kept on ice until analysis using the LSR II. Data analysis was performed using the FlowJo software, and the MFI was used to determine antibody internalization. All data analyses were performed using GraphPad Prism version 7.02 for Windows (GraphPad Software).

PD-1 Receptor Downregulation Analyses

To determine the effect of antibody internalization on surface PD-1 levels, CHO $PD\text{-}1^+CTLA4^+$ (10:1) or primary $CD3^+$ T cells stimulated with 1 μg/mL of anti-CD3 antibody (clone OKT3, BioLegend) alone or in combination with 5 μg/mL anti-CD28 antibody (clone 28.2, BioLegend) were incubated with serial dilutions of control and test antibodies, starting at a concentration of 180 nmol/L. Cells were added at 5×10^5 and 1×10^6 cells/well for CHO and primary $CD3^+$ T cells, respectively, followed by incubation at 37°C with 5% CO_2 for time intervals noted. For Time 0 controls, cells were incubated at 4°C for 30 minutes. After incubation, cells were washed twice with FACS buffer to remove excess antibody, and residual surface PD-1 receptor was detected by incubation with 50 μg/mL of a noncompeting anti–PD-1 antibody labeled with allophycocyanin at 4°C for 30 minutes. Primary $CD3^+$ T cells were additionally costained with fluorescently labeled anti-CD4 (clone RPA-T4, BioLegend) and anti-CD8 (clone RPA-T8, BioLegend) antibodies, in addition to propidium iodide (Sigma) to exclude dead cells. After staining, CHO cells were fixed with 4% PFA for 10 minutes, and T cells were kept on ice until analysis using an LSR II flow cytometer (BD Biosciences). Data analysis was performed using the FlowJo software, and residual cell-surface PD-1 was measured as the MFI of allophycocyanin signal. All data analyses were performed using GraphPad Prism version 7.02 for Windows (GraphPad Software).

Receptor Tracking by High Content Imaging

Receptor $PD\text{-}1^+$SNAP-tag/$CTLA4^+$CLIP-tag double-positive CHO cells were labeled with 2 μmol/L Cell Tracker red CMTPX, plated at 2×10^4 cells/well in a 96-well plate, and incubated overnight at 37°C. Receptors were prelabeled with SNAP-Cell 647 and CLIP-Cell 505 according to the manufacturer's instructions (New England Bio Labs). Briefly, cells were incubated with 1:200 SNAP-Cell 647 and 1:200 CLIP-Cell 505 in complete media at 37°C for 60 minutes. After three washes, cells were incubated with 2 μg/mL Hoechst for 30 minutes. After three washes, cells were resuspended in complete media. Immediately after addition of 40 nmol/L MEDI5752, anti–PD-1, anti-CTLA4, mvPD-1, or mvCTLA4 mAb treatment, cells were imaged. This staining procedure was used for total PD-1 receptor and CTLA4 receptor turnover quantitation and colocalization analysis.

PD-1 Receptor, CTLA4 Receptor, and Lysosome Colocalization

Receptor $PD\text{-}1^+$SNAP-tag/$CTLA4^+$CLIP-tag double-positive CHO cells were labeled with 20 μmol/L Cell Tracker blue CMAC (Molecular Probes), plated at 2×10^4 cells/well in a 96-well plate, and incubated

overnight at 37°C. The next day, cells were incubated with 1:200 SNAP-Cell TMR, 1:200 CLIP-Cell 505, and 50 nmol/L LysoTracker Red (Invitrogen) in complete media at 37°C for 60 minutes. After three washes, cells were resuspended in complete media. Immediately after addition of 40 nmol/L MEDI5752, anti–PD-1, anti-CTLA4, mvPD-1, or mvCTLA4 mAb treatment, cells were imaged.

PD-1 Receptor, Drug, and Lysosome Colocalization

Receptor PD-1^{+}SNAP-tag/CTLA4^{+}CLIP-tag double-positive CHO cells were labeled with 20 μmol/L Cell Tracker blue CMAC, plated at 2×10^4 cells/well in a 96-well plate, and incubated overnight at 37°C. The next day, cells were incubated with 1:200 SNAP-Cell TMR and 50 nmol/L LysoTracker Red (Invitrogen) in complete media at 37°C for 60 minutes. After three washes, cells were resuspended in complete media. Immediately after addition of 40 nmol/L Alexa Fluor 488–labeled MEDI5752 or 40 nmol/L Alexa Fluor 488–labeled anti-PD-1 mAb treatment, cells were imaged.

MCA205 Tumor Model

Antitumor activity of MEDI5752 was assessed in a novel transgenic mouse strain generated by genOway that expresses human PD-1 and CTLA4 instead of the murine proteins (C57BL/6N-*Pdcd1*^{tm1}(hu*PDCD1*-ICP11)Geno *Ctla4*^{tm1}(hu*CTLA4*-ICP13)Geno). This mouse strain was developed by intercrossing the human PD-1 (C57BL/6N-*Pdcd1*^{tm1}(hu*PDCD1*-ICP11)Geno) and the human CTLA4 (C57BL/6N-*Ctla4*^{tm1}(hu*CTLA4*-ICP13)Geno) mouse strains. Briefly, the human PD-1 strain was developed by inserting within the mouse PD-1 locus a chimeric PD-1 with a human extracellular domain and murine transmembrane and intracellular domains. Similarly, the human CTLA4 strain was developed by inserting within the mouse CTLA4 locus a chimeric CTLA4 with a human extracellular domain and murine transmembrane and intracellular domains. For both strains, homologous recombination was performed in C57BL/6N-derived embryonic stem cells, and mouse chimeras were bred with Cre (for the human PD-1 strain) and Flp (for the human CTLA4 strain) delete mice to excise the neomycin selection cassette and generate heterozygous mice carrying the neoexcised humanized knock-in alleles. The mice were bred at Charles River France, supplied at 6 to 8 weeks of age and >17 g, and housed under specific pathogen-free conditions in Tecniplast Green Line IVC Sealsafe cages holding a maximum of six animals with irradiated aspen chip bedding, Nestlets nesting material, a cardboard tunnel, and wooden chew blocks. Mice were housed on a 12/12 light/dark cycle, with *ad libitum* UV-treated water and RM1 rodent diet. 100 μL containing 5×10^5 MCA205 cells in 50% growth factor–reduced Matrigel (Corning) were s.c. injected into the right flanks of the mice. Cells did not undergo any *in vivo* passaging and were maintained under limited passage from original stocks (typically under 5). To reduce immunogenic responses to dosing of human antibodies, mice were i.v. injected with 10 mg/kg anti-CD20 rIgG2b antibody (BioLegend) 5 or 6 days after tumor implantation in order to deplete B cells. Mice were then i.p. injected with MEDI5752, anti–PD-1, anti-CTLA4, or isotype hIgG mAbs either both on days 7 and 11, or only on day 11 after tumor implantation. Tumor volume was measured 3 times per week with calipers using the formula (width^2 × length)/2. Mice were sacrificed when they reached humane welfare limits pertaining to tumor volume (average diameter of 15 mm) or tumor condition (ulceration of the skin above the tumor). Survival was defined as the time to reach this welfare endpoint. These studies were performed in accordance with the UK Animal (Scientific Procedures) Act 1986 and the EU Directive 86/609, under a UK Home Office Project License, using guidelines outlined by Workman and colleagues (59).

Radiolabeled Biodistribution Study

MEDI5752, anti–PD-1, anti-CTLA4, and isotype mAbs were radiolabeled with ^{89}Zr by the Wolfson Molecular Imaging Centre (UK). PD-1^{huKI}/CTLA4^{huKI} mice bearing subcutaneous MCA205 tumors (100 μL containing 5×10^4 MCA205 cells in 50% growth factor–reduced Matrigel) were i.v. injected 15 days after tumor implantation with ^{89}Zr-labeled antibodies, and the injected dose was calculated as the difference in radioactivity in the syringe before and after injection after decay correction to the time of injection. Mice injected with ^{89}Zr-labeled anti-CTLA4 antibody were also i.p. injected with the same dose level of unlabeled anti–PD-1 antibody, and mice injected with ^{89}Zr-labeled anti–PD-1 antibody were also i.p. injected with the same dose level of unlabeled anti-CTLA4 antibody to account for any biological effects of dual PD-1 and CTLA4 blockade. Mice were anesthetized and underwent a static 20-minute PET scan at the indicated timepoints after dosing using a Siemens Inveon PET scanner. Images were segmented to determine tracer uptake in the tumor and measure the meanSUV for each animal. Ninety-six hours after dosing, animals were sacrificed and bled, and tissues were harvested, weighed, and analyzed using a Perkin Elmer Wallac Wizard Gamma counter. These data were used to calculate the tissue:blood ratio of the ^{89}Zr signal. To normalize for levels of antibody in the blood, the tumor imaging data were expressed as the ratio of meanSUV:blood.

OE21 10xGS Tumor Model

The human tumor cell line OE21 was transduced to express a construct containing six viral peptides (three EBV-derived peptides, two influenza A–derived peptides, and one CMV-derived peptide) with $(GS)_{10}$ linkers under an EF1 promoter sequence. Healthy donor PBMC from HLA-A2^{+} donors were incubated in a 1:1 mixture of RPMI-1640 and AIM-V media supplemented with 5% human serum and 50 IU/mL IL2 for 11 days with 1 μg/mL influenza A–derived peptide GILGFVFTL (MBL) to expand the CD8^{+} peptide-reactive T cells. 100 μL containing 2×10^6 OE21-10xGS cells in 50% Matrigel (Corning) were s.c. injected into the flank of NSG mice (The Jackson Laboratory). All animals were housed per Institutional Animal Care and Use Committee–approved protocols in the Laboratory Animal Resources facility, an Association for Animal Accreditation of Laboratory Animal Care and United States Department of Agriculture–licensed facility. The animals were kept in sterile microisolator units, provided with sterile bedding and food, and acidified drinking water *ad libitum*. Environmental conditions were standardized (room temperature: 20°C ± 1°C; relative humidity: 50% ± 10%; 12-hour light–dark cycle). Seven days after tumor implantation, mice were i.v. injected with 1×10^6 peptide-stimulated antigen-specific CD8^{+} T cells and then i.p. injected with 10 mg/kg MEDI5752, anti–PD-1, anti-CTLA4, or an isotype hIgG on days 9, 11, 14, and 17 after tumor implantation. Two to 3 hours prior to this treatment, mice were i.p. injected with a combination of 100 mg/kg GammaGard (Shire Labs) and 20 mg/kg of anti-mouse CD16/CD32 (BioXCell). PBMC were obtained from healthy donors and prescreened for HLA haplotype and viral peptide reactivity in accordance with the Declaration of Helsinki, with donors signing a written informed consent before sample collection.

Clinical Study

The first-time-in-human clinical study (NCT03530397) was approved by appropriate Institutional Review Boards at each participating site and conducted in accordance with Good Clinical Practice guidelines and the ethical principles of the Declaration of Helsinki. All patients provided written informed consent. Escalating doses of MEDI5752 were administered i.v. Safety was assessed using CTCAE v4.03. Response assessment was done utilizing RECISTv1.1. The study is ongoing.

Statistical Analysis

In two-cell reporter assays, potency was determined by generating EC_{50} values using a nonlinear regression model [log agonist vs. response – variable slope (four parameters)]. Statistical significance

for MEDI5752 versus control groups in primary human anti-CD3/SEB assays was determined using a paired *t* test and in Treg suppression assays was determined using a two-way ANOVA with Dunnett multiple comparisons post test. Statistical significance for MEDI5752 versus control groups was determined for tumor imaging and tumor volume using a mixed-effects model with the Geisser–Greenhouse correction and for gamma counting using an ordinary one-way ANOVA, both with Dunnett multiple comparisons testing. For survival analysis, statistical significance was determined using the log-rank test, and for the dose-dependent effects of MEDI5752 on tumor volume, statistical significance was determined using a mixed-effects model with the Geisser–Greenhouse correction and Tukey multiple comparisons testing. For all tests, significance was determined with a 95% confidence interval ($P > 0.05$; *, $P < 0.05$; **, $P < 0.01$; ***, $P < 0.001$; ****, $P < 0.0001$) on GraphPad Prism, version 8.

Authors' Disclosures

S.J. Dovedi reports personal fees from AstraZeneca during the conduct of the study and outside the submitted work; in addition, S.J. Dovedi has a patent for 10,457,732 issued to AstraZeneca. M.J. Elder reports being an AstraZeneca employee outside the submitted work. J. Hair reports personal fees and other support from AstraZeneca Ltd. during the conduct of the study. S.-A. Im reports grants and other support from AstraZeneca, Eisai, Pfizer, and Roche; other support from Amgen, Lilly, Hanmi, MSD, and Novartis; and grants from Daewoong outside the submitted work. B. Tran reports other support from AstraZeneca during the conduct of the study; and grants and personal fees from Amgen, AstraZeneca, Astellas, BMS, Janssen, Pfizer, MSD, Ipsen, and Bayer, and personal fees from IQVIA, Sanofi, Tolmar, Novartis, and Roche outside the submitted work. D.S. Subramaniam reports other support from AstraZeneca Plc during the conduct of the study. S.D. Gainer reports other support from GlaxoSmithKline and Novartis, and personal fees and other support from AstraZeneca outside the submitted work. K. Vashisht reports being employee of AstraZeneca and receiving compensation from them. A. Lewis reports other support from AstraZeneca during the conduct of the study and outside the submitted work. Y. Wang reports personal fees from AstraZeneca outside the submitted work. M.G. Overstreet reports personal fees from Acea Biosciences outside the submitted work. J. Dodgson reports personal fees from AstraZeneca outside the submitted work. M. Morrow reports other support from F-star Therapeutics outside the submitted work; in addition, M. Morrow has a patent for US 10,457,732 issued. G.J. Rainey reports other support from Gritstone Oncology, Immetas Therapeutics, Life Biosciences, and Mabvax Therapeutics Holdings, Inc., and personal fees from Cambridge Healthtech Institute outside the submitted work; in addition, G.J. Rainey has a patent for bispecific binding proteins and uses thereof issued. G.J. Browne reports other support from AstraZeneca during the conduct of the study and outside the submitted work. T.V. Murray reports personal fees and other support from AstraZeneca outside the submitted work. W. Dall'Acqua reports working for, and receiving a salary from, AstraZeneca. I. Achour reports other support from AstraZeneca during the conduct of the study and outside the submitted work. D.J. Freeman reports personal fees from AstraZeneca during the conduct of the study and outside the submitted work; in addition, D.J. Freeman reports being a full-time employee and shareholder of AstraZeneca. R.W. Wilkinson reports other support from AstraZeneca during the conduct of the study and outside the submitted work. No disclosures were reported by the other authors.

Authors' Contributions

S.J. Dovedi: Conceptualization, formal analysis, supervision, validation, investigation, visualization, methodology, writing–original draft, project administration, writing–review and editing. **B. Wang:** Investigation, methodology. **S.-A. Im:** Investigation, writing–review and editing. **B. Tran:** Investigation, writing–review and editing. **D.S. Subramaniam:** Formal analysis, investigation, methodology, writing–original draft, writing–review and editing. **S.D. Gainer:** Formal analysis, investigation, methodology, writing–original draft, writing–review and editing. **K. Vashisht:** Formal analysis, investigation, visualization, methodology, writing–original draft. **A. Lewis:** Formal analysis, investigation, visualization, methodology. **X. Jin:** Investigation, visualization, methodology. **S. Kentner:** Investigation, visualization, methodology. **K. Mulgrew:** Investigation, methodology. **M.J. Elder:** Formal analysis, investigation, methodology, writing–original draft, writing–review and editing. **Y. Wang:** Investigation, methodology. **M.G. Overstreet:** Investigation, methodology. **J. Dodgson:** Formal analysis, investigation, methodology. **Y. Wu:** Investigation, methodology. **A. Palazon:** Investigation, methodology. **M. Morrow:** Conceptualization, investigation. **G.J. Rainey:** Conceptualization, investigation. **G.J. Browne:** Investigation, visualization, methodology. **F. Neal:** Investigation, visualization, methodology. **T.V. Murray:** Investigation, methodology. **C. Yang:** Formal analysis, investigation, methodology. **A.D. Toloczko:** Investigation, visualization, methodology. **W. Dall'Acqua:** Resources, supervision. **I. Achour:** Formal analysis, investigation, visualization, methodology, writing–original draft. **D.J. Freeman:** Supervision, investigation, writing–original draft. **R.W. Wilkinson:** Resources, supervision, investigation, writing–original draft. **Y. Mazor:** Conceptualization, formal analysis, supervision, investigation, visualization, methodology, writing–original draft, writing–review and editing. **S.I. Sitnikova:** Formal analysis, investigation, visualization, methodology, writing–original draft, writing–review and editing. **L. Irving:** Investigation, visualization, methodology. **A. Hansen:** Investigation, methodology. **J. Hair:** Formal analysis, investigation, visualization, methodology, writing–original draft. **D.C. Jones:** Investigation, methodology. **S. Hasani:** Investigation, methodology.

Acknowledgments

The authors would like to thank Janette Dillon, Emily Dick, and Natalie Tigue for generating the CHO K1 OKT3-CD14 (low) hB7H1 (high) cl 2 cells.

Received October 13, 2020; revised December 4, 2020; accepted December 17, 2020; published first January 8, 2021.

REFERENCES

1. Wei SC, Duffy CR, Allison JP. Fundamental mechanisms of immune checkpoint blockade therapy. Cancer Discov 2018;8:1069–86.
2. Atkins MB, Clark JI, Quinn DI. Immune checkpoint inhibitors in advanced renal cell carcinoma: experience to date and future directions. Ann Oncol 2017;28:1484–94.
3. Larkin J, Chiarion-Sileni V, Gonzalez R, Grob JJ, Cowey CL, Lao CD, et al. Combined nivolumab and ipilimumab or monotherapy in untreated melanoma. N Engl J Med 2015;373:23–34.
4. Hellmann MD, Paz-Ares L, Bernabe Caro R, Zurawski B, Kim SW, Carcereny Costa E, et al. Nivolumab plus ipilimumab in advanced non-small-cell lung cancer. N Engl J Med 2019;381:2020–31.
5. Larkin J, Chiarion-Sileni V, Gonzalez R, Grob JJ, Rutkowski P, Lao CD, et al. Five-year survival with combined nivolumab and ipilimumab in advanced melanoma. N Engl J Med 2019;381:1535–46.
6. Motzer RJ, Tannir NM, McDermott DF, Aren Frontera O, Melichar B, Choueiri TK, et al. Nivolumab plus ipilimumab versus sunitinib in advanced renal-cell carcinoma. N Engl J Med 2018;378:1277–90.
7. Ascierto PA, Del Vecchio M, Robert C, Mackiewicz A, Chiarion-Sileni V, Arance A, et al. Ipilimumab 10 mg/kg versus ipilimumab 3 mg/kg in patients with unresectable or metastatic melanoma: a randomised, double-blind, multicentre, phase 3 trial. Lancet Oncol 2017;18:611–22.
8. Wolchok JD, Neyns B, Linette G, Negrier S, Lutzky J, Thomas L, et al. Ipilimumab monotherapy in patients with pretreated advanced

melanoma: a randomised, double-blind, multicentre, phase2, dose-ranging study. Lancet Oncol 2010;11:155–64.
9. Gros A, Robbins PF, Yao X, Li YF, Turcotte S, Tran E, et al. PD-1 identifies the patient-specific CD8(+) tumor-reactive repertoire infiltrating human tumors. J Clin Invest 2014;124:2246–59.
10. Freeman GJ, Long AJ, Iwai Y, Bourque K, Chernova T, Nishimura H, et al. Engagement of the PD-1 immunoinhibitory receptor by a novel B7 family member leads to negative regulation of lymphocyte activation. J Exp Med 2000;192:1027–34.
11. Latchman Y, Wood CR, Chernova T, Chaudhary D, Borde M, Chernova I, et al. PD-L2 is a second ligand for PD-1 and inhibits T cell activation. Nat Immunol 2001;2:261–8.
12. Hui E, Cheung J, Zhu J, Su X, Taylor MJ, Wallweber HA, et al. T cell costimulatory receptor CD28 is a primary target for PD-1-mediated inhibition. Science 2017;355:1428–33.
13. Kamphorst AO, Wieland A, Nasti T, Yang S, Zhang R, Barber DL, et al. Rescue of exhausted CD8 T cells by PD-1-targeted therapies is CD28-dependent. Science 2017;355:1423–7.
14. Walunas TL, Lenschow DJ, Bakker CY, Linsley PS, Freeman GJ, Green JM, et al. CTLA-4 can function as a negative regulator of T cell activation. Immunity 1994;1:405–13.
15. Fallarino F, Fields PE, Gajewski TF. B7-1 engagement of cytotoxic T lymphocyte antigen 4 inhibits T cell activation in the absence of CD28. J Exp Med 1998;188:205–10.
16. Krummel MF, Allison JP. CD28 and CTLA-4 have opposing effects on the response of T cells to stimulation. J Exp Med 1995;182:459–65.
17. Masteller EL, Chuang E, Mullen AC, Reiner SL, Thompson CB. Structural analysis of CTLA-4 function in vivo. J Immunol 2000;164:5319–27.
18. Peggs KS, Quezada SA, Chambers CA, Korman AJ, Allison JP. Blockade of CTLA-4 on both effector and regulatory T cell compartments contributes to the antitumor activity of anti-CTLA-4 antibodies. J Exp Med 2009;206:1717–25.
19. van der Merwe PA, Bodian DL, Daenke S, Linsley P, Davis SJ. CD80 (B7-1) binds both CD28 and CTLA-4 with a low affinity and very fast kinetics. J Exp Med 1997;185:393–403.
20. Qureshi OS, Kaur S, Hou TZ, Jeffery LE, Poulter NS, Briggs Z, et al. Constitutive clathrin-mediated endocytosis of CTLA-4 persists during T cell activation. J Biol Chem 2012;287:9429–40.
21. Qureshi OS, Zheng Y, Nakamura K, Attridge K, Manzotti C, Schmidt EM, et al. Trans-endocytosis of CD80 and CD86: a molecular basis for the cell-extrinsic function of CTLA-4. Science 2011;332:600–3.
22. Ahmadzadeh M, Johnson LA, Heemskerk B, Wunderlich JR, Dudley ME, White DE, et al. Tumor antigen-specific CD8 T cells infiltrating the tumor express high levels of PD-1 and are functionally impaired. Blood 2009;114:1537–44.
23. Montler R, Bell RB, Thalhofer C, Leidner R, Feng Z, Fox BA, et al. OX40, PD-1 and CTLA-4 are selectively expressed on tumor-infiltrating T cells in head and neck cancer. Clin Transl Immunology 2016;5:e70.
24. Walker LS, Sansom DM. The emerging role of CTLA-4 as a cell-extrinsic regulator of T cell responses. Nat Rev Immunol 2011;11:852–63.
25. Tanaka A, Sakaguchi S. Regulatory T cells in cancer immunotherapy. Cell Res 2017;27:109–18.
26. Gide TN, Quek C, Menzies AM, Tasker AT, Shang P, Holst J, et al. Distinct immune cell populations define response to anti-PD-1 monotherapy and anti-PD-1/anti-CTLA-4 combined therapy. Cancer Cell 2019;35:238–55.
27. Siddiqui I, Schaeuble K, Chennupati V, Fuertes Marraco SA, Calderon-Copete S, Pais Ferreira D, et al. Intratumoral Tcf1(+)PD-1(+)CD8(+) T cells with stem-like properties promote tumor control in response to vaccination and checkpoint blockade immunotherapy. Immunity 2019;50:195–211.
28. Fransen MF, van der Sluis TC, Ossendorp F, Arens R, Melief CJ. Controlled local delivery of CTLA-4 blocking antibody induces CD8+ T-cell-dependent tumor eradication and decreases risk of toxic side effects. Clin Cancer Res 2013;19:5381–9.
29. Hebb JPO, Mosley AR, Vences-Catalan F, Rajasekaran N, Rosen A, Ellmark P, et al. Administration of low-dose combination anti-CTLA4, anti-CD137, and anti-OX40 into murine tumor or proximal to the tumor draining lymph node induces systemic tumor regression. Cancer Immunol Immunother 2018;67:47–60.
30. Marabelle A, Kohrt H, Sagiv-Barfi I, Ajami B, Axtell RC, Zhou G, et al. Depleting tumor-specific Tregs at a single site eradicates disseminated tumors. J Clin Invest 2013;123:2447–63.
31. Pai CS, Simons DM, Lu X, Evans M, Wei J, Wang YH, et al. Tumor-conditional anti-CTLA4 uncouples antitumor efficacy from immunotherapy-related toxicity. J Clin Invest 2019;129:349–63.
32. Sandin LC, Eriksson F, Ellmark P, Loskog AS, Totterman TH, Mangsbo SM. Local CTLA4 blockade effectively restrains experimental pancreatic adenocarcinoma growth in vivo. Oncoimmunology 2014;3:e27614.
33. Simmons AD, Moskalenko M, Creson J, Fang J, Yi S, VanRoey MJ, et al. Local secretion of anti-CTLA-4 enhances the therapeutic efficacy of a cancer immunotherapy with reduced evidence of systemic autoimmunity. Cancer Immunol Immunother 2008;57:1263–70.
34. Tselikas L, de Baere T, Isoardo T, Susini S, Ser-Le Roux K, Polrot M, et al. Pickering emulsions with ethiodized oil and nanoparticles for slow release of intratumoral anti-CTLA4 immune checkpoint antibodies. J Immunother Cancer 2020;8:e000579.
35. Tuve S, Chen BM, Liu Y, Cheng TL, Toure P, Sow PS, et al. Combination of tumor site-located CTL-associated antigen-4 blockade and systemic regulatory T-cell depletion induces tumor-destructive immune responses. Cancer Res 2007;67:5929–39.
36. van Hooren L, Sandin LC, Moskalev I, Ellmark P, Dimberg A, Black P, et al. Local checkpoint inhibition of CTLA-4 as a monotherapy or in combination with anti-PD1 prevents the growth of murine bladder cancer. Eur J Immunol 2017;47:385–93.
37. Cha E, Klinger M, Hou Y, Cummings C, Ribas A, Faham M, et al. Improved survival with T cell clonotype stability after anti-CTLA-4 treatment in cancer patients. Sci Transl Med 2014;6:238ra70.
38. Oh DY, Cham J, Zhang L, Fong G, Kwek SS, Klinger M, et al. Immune toxicities elicted by CTLA-4 blockade in cancer patients are associated with early diversification of the T-cell repertoire. Cancer Res 2017;77:1322–30.
39. Duhen T, Duhen R, Montler R, Moses J, Moudgil T, de Miranda NF, et al. Co-expression of CD39 and CD103 identifies tumor-reactive CD8 T cells in human solid tumors. Nat Commun 2018;9:2724.
40. Mazor Y, Oganesyan V, Yang C, Hansen A, Wang J, Liu H, et al. Improving target cell specificity using a novel monovalent bispecific IgG design. MAbs 2015;7:377–89.
41. Oganesyan V, Gao C, Shirinian L, Wu H, Dall'Acqua WF. Structural characterization of a human Fc fragment engineered for lack of effector functions. Acta Crystallogr D Biol Crystallogr 2008;64:700–4.
42. Rhoden JJ, Dyas GL, Wroblewski VJ. A modeling and experimental investigation of the effects of antigen density, binding affinity, and antigen expression ratio on bispecific antibody binding to cell surface targets. J Biol Chem 2016;291:11337–47.
43. Claus C, Ferrara C, Xu W, Sam J, Lang S, Uhlenbrock F, et al. Tumor-targeted 4–1BB agonists for combination with T cell bispecific antibodies as off-the-shelf therapy. Sci Transl Med 2019;11:eaav5989.
44. Trang VH, Zhang X, Yumul RC, Zeng W, Stone IJ, Wo SW, et al. A coiled-coil masking domain for selective activation of therapeutic antibodies. Nat Biotechnol 2019;37:761–5.
45. Waite JC, Wang B, Haber L, Hermann A, Ullman E, Ye X, et al. Tumor-targeted CD28 bispecific antibodies enhance the antitumor efficacy of PD-1 immunotherapy. Sci Transl Med 2020;12:eaba2325.
46. Arce Vargas F, Furness AJS, Litchfield K, Joshi K, Rosenthal R, Ghorani E, et al. Fc effector function contributes to the activity of human anti-CTLA-4 antibodies. Cancer Cell 2018;33:649–63.
47. Sharma A, Subudhi SK, Blando J, Scutti J, Vence L, Wargo J, et al. Anti-CTLA-4 immunotherapy does not deplete FOXP3(+) regulatory T cells (Tregs) in human cancers. Clin Cancer Res 2019;25:1233–8.
48. Guo X, Zhang Y, Zheng L, Zheng C, Song J, Zhang Q, et al. Global characterization of T cells in non-small-cell lung cancer by single-cell sequencing. Nat Med 2018;24:978–85.
49. Kvistborg P, Philips D, Kelderman S, Hageman L, Ottensmeier C, Joseph-Pietras D, et al. Anti-CTLA-4 therapy broadens the melanoma-reactive CD8+ T cell response. Sci Transl Med 2014;6:254ra128.

50. Spranger S, Dai D, Horton B, Gajewski TF. Tumor-residing Batf3 dendritic cells are required for effector T cell trafficking and adoptive T cell therapy. Cancer Cell 2017;31:711–23.
51. Mayoux M, Roller A, Pulko V, Sammicheli S, Chen S, Sum E, et al. Dendritic cells dictate responses to PD-L1 blockade cancer immunotherapy. Sci Transl Med 2020;12:eaav7431.
52. Harms BD, Kearns JD, Iadevaia S, Lugovskoy AA. Understanding the role of cross-arm binding efficiency in the activity of monoclonal and multispecific therapeutic antibodies. Methods 2014;65:95–104.
53. Hatterer E, Barba L, Noraz N, Daubeuf B, Aubry-Lachainaye JP, von der Weid B, et al. Co-engaging CD47 and CD19 with a bispecific antibody abrogates B-cell receptor/CD19 association leading to impaired B-cell proliferation. MAbs 2019;11:322–34.
54. Jarantow SW, Bushey BS, Pardinas JR, Boakye K, Lacy ER, Sanders R, et al. Impact of cell-surface antigen expression on target engagement and function of an epidermal growth factor receptor x c-MET bispecific antibody. J Biol Chem 2015;290:24689–704.
55. Mazor Y, Hansen A, Yang C, Chowdhury PS, Wang J, Stephens G, et al. Insights into the molecular basis of a bispecific antibody's target selectivity. MAbs 2015;7:461–9.
56. Mazor Y, Sachsenmeier KF, Yang C, Hansen A, Filderman J, Mulgrew K, et al. Enhanced tumor-targeting selectivity by modulating bispecific antibody binding affinity and format valence. Sci Rep 2017;7:40098.
57. Schubert I, Saul D, Nowecki S, Mackensen A, Fey GH, Oduncu FS. A dual-targeting triplebody mediates preferential redirected lysis of antigen double-positive over single-positive leukemic cells. MAbs 2014;6:286–96.
58. Zheng S, Moores S, Jarantow S, Pardinas J, Chiu M, Zhou H, et al. Cross-arm binding efficiency of an EGFR x c-Met bispecific antibody. MAbs 2016;8:551–61.
59. Workman P, Aboagye EO, Balkwill F, Balmain A, Bruder G, Chaplin DJ, et al. Guidelines for the welfare and use of animals in cancer research. Br J Cancer 2010;102:1555–77.